

# Human-Activity AGV Quality Assessment: A Benchmark Dataset and an Objective Evaluation Metric

Zhichao Zhang<sup>1</sup> Wei Sun<sup>1</sup> Xinyue Li<sup>1</sup> Yunhao Li<sup>1</sup> Qihang Ge<sup>1</sup> Jun Jia<sup>1</sup> Zicheng Zhang<sup>1</sup>  
Zhongpeng Ji<sup>2</sup> Fengyu Sun<sup>2</sup> Shangling Jui<sup>2</sup> Xionghuo Min<sup>1</sup> Guangtao Zhai<sup>1</sup>

<sup>1</sup>Shanghai Jiao Tong University, Shanghai, China

<sup>2</sup>Huawei Technologies, Shanghai, China

## Abstract

AI-driven video generation techniques have made significant progress in recent years. However, AI-generated videos (AGVs) involving human activities often exhibit substantial visual and semantic distortions, hindering the practical application of video generation technologies in real-world scenarios. To address this challenge, we conduct a pioneering study on human activity AGV quality assessment, focusing on visual quality evaluation and the identification of semantic distortions. First, we construct the AI-Generated Human activity Video Quality Assessment (Human-AGVQA) dataset, consisting of 3,200 AGVs derived from 8 popular text-to-video (T2V) models using 400 text prompts that describe diverse human activities. We conduct a subjective study to evaluate the **human appearance quality, action continuity quality, and overall video quality** of AGVs, and identify semantic issues of human body parts. Based on Human-AGVQA, we benchmark the performance of T2V models and analyze their strengths and weaknesses in generating different categories of human activities. Second, we develop an objective evaluation metric, named AI-Generated Human activity Video Quality metric (GHVQ), to automatically analyze the quality of human activity AGVs. GHVQ systematically extracts human-focused quality features, AI-generated content-aware quality features, and temporal continuity features, making it a comprehensive and explainable quality metric for human activity AGVs. The extensive experimental results show that GHVQ outperforms existing quality metrics on the Human-AGVQA dataset by a large margin, demonstrating its efficacy in assessing the quality of human activity AGVs. The Human-AGVQA dataset and GHVQ metric will be released in public at [GitHub](#).

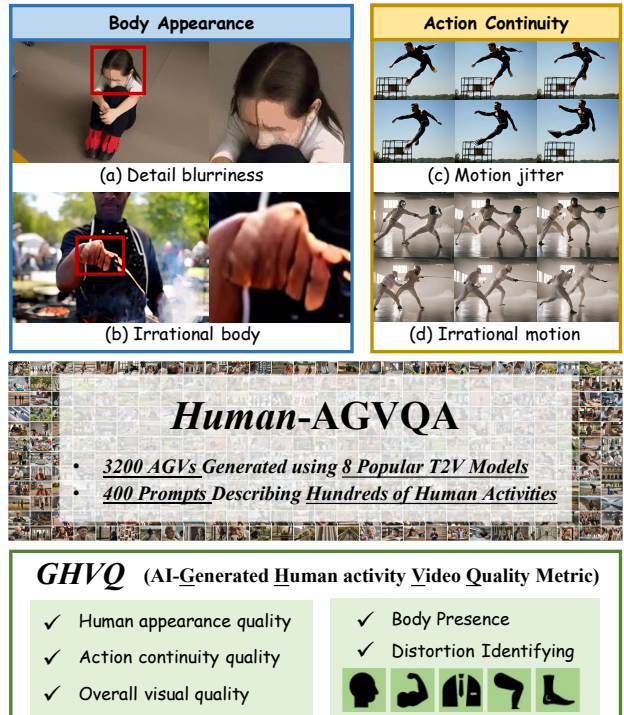


Figure 1. Overview of this work. This study aims to address the distortions in human activity AGVs, with some typical distortions shown in the first row. To achieve this goal, we introduce the Human-AGVQA dataset, consisting of 3,200 human activity AGVs with the quality labels, and the GHVQ metric to objectively compute the quality of human activity AGVs.

## 1. Introduction

AI-driven video generation, particularly in the form of text-to-video (T2V) generation [1, 9], can automatically create visual realism videos according to text descriptions. This convenient and cost-effective method of video creation has significant potential for applications in entertainment, art, advertising, education, and various other fields. However,

many studies [33, 53] indicate that current T2V models still struggle to generate realistic human figures and actions. For instance, AI-generated videos (AGVs) may exhibit distorted, incomplete, or abnormal body parts and actions, as illustrated in Figure 1. These artifacts can significantly affect the user’s perceptual quality, as the human body is highly structured, and the human visual system is susceptible to irregular body form and movement irregularities.

Therefore, accurately assessing the quality of human-activity AGVs is critical to automatically monitor the visual quality of large-scale AGVs in video generation applications, measure the progress of T2V models, and serve as an optimization or reward function to enhance the capability of T2V models. Unfortunately, the quality assessment for AI-generated content (AIGC) [54] is still in its infancy. The general image/video quality assessment (I/VQA) metrics have been shown to perform poorly in evaluating AGVs [39, 84], while common used metrics in T2V studies, such as Inception Score (IS) [65], Fréchet Inception Distance (FID) [28], and Fréchet Video Distance (FVD) [79], evaluate the generation performance and diversity of T2V models by comparing a set of AGVs to real data distributions in feature Inception feature spaces, thus failing to reflect the quality at the individual video level.

To bridge this gap, we establish the first quality assessment benchmark for human activity AGVs, providing a comprehensive analysis of quality issues in human activity videos generated by mainstream T2V models and serving as a testbed for validating the effectiveness of quality assessment metrics in evaluating human activity AGVs. Specifically, we first construct the AI-Generated Human activity Video Quality Assessment (Human-AGVQA) dataset, which contains 3,200 AGVs derived by 8 state-of-the-art T2V models using 400 text prompts. We define two practical quality assessment problems for human activity AGVs. The first is quality scoring, which quantifies the specific quality score of AGVs, allowing us to compare the quality of one AGV or T2V model against others. The second one is semantic issue identification, which pinpoints problematic body parts that affect quality scores, providing insights for further optimization of T2V models. Therefore, for the quality scoring task, we invite 80 subjects to rate the quality scores of AGVs based on three critical dimensions: human appearance quality, action continuity quality, and overall visual quality. For the semantic issue identification task, we invite 5 experts to label whether the human bodies (*face, arms, torso, legs, and feet*) exhibit semantic issues. Based on these subjectively rated quality labels, we can benchmark the performance of T2V models and analyze their strengths and weaknesses in generating different categories of human activities.

To address the lack of objective metrics for assessing the quality of human activity AGVs, we propose the *AI-*

*Generated Human activity Video Quality metric (GHVQ)* to automatically evaluate the quality scores of human activity AGVs and identifies their semantic issues. Specifically, GHVQ consists of a spatial quality analyzer, an action quality analyzer, a text feature extractor, and a quality regressor. The spatial quality analyzer extracts human-focused and holistic quality features at the frame level. For human-focused features, we employ body-part segment masks to explicitly extract human body part-aware features, followed by an inner-body distortion analysis module and a cross-body distortion analysis module to refine these features at the individual body part level and the body part interaction level, respectively. Holistic quality features are extracted using a pre-trained AIGC IQA method to better represent complex AIGC artifacts. The action quality analyzer captures the temporal continuity of AGVs using a pre-trained action recognition model. To ensure semantic alignment, the text feature extractor is employed to capture text-based semantic features. Finally, the four types of features are concatenated to form quality-aware feature representations. Two multi-layer perceptrons (MLPs) are used to simultaneously predict quality scores and binary decisions for each assessment dimension. Experimental results demonstrate that GHVQ outperforms existing metrics across all evaluated quality dimensions on the Human-AGVQA dataset, highlighting its effectiveness as a comprehensive metric for assessing the quality of complex human activity AGVs. We summarize the contributions of this paper as:

- We establish the *Human-AGVQA* dataset for assessing the quality of human activity AGVs. *Human-AGVQA* comprises 3,200 videos generated by 8 T2V models using 400 text prompts, along with subjectively rated quality labels for 2 types of assessment tasks. The diversity of text prompts and the richness of quality labels make our benchmark well-suited for investigating the quality assessment of human activity AGVs.
- We propose the GHVQ metric to automatically evaluate the human appearance quality, action continuity quality, and overall video quality of AGVs, and identify whether five human body parts exhibit semantic issues. Experimental results indicate that GHVQ significantly outperforms existing related quality metrics, demonstrating its effectiveness.

## 2. Related Works

**Video Generation Techniques** can be broadly categorized into three types: GAN/VAE-based methods [14, 46, 59, 62], autoregressive-based methods [3, 20, 31, 49, 80, 86], and diffusion-based methods [7, 8, 25, 29, 30, 35, 67, 90, 94, 100, 104]. Among these, diffusion-based methods have seen significant progress, with some commercial models [1, 16] already being developed or launched for real-world applications. However, several studies [13, 33, 53, 70]

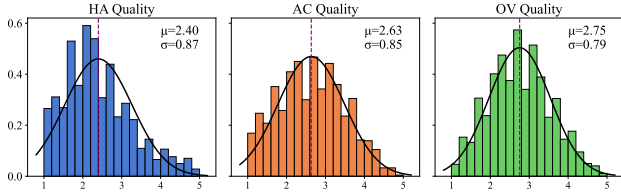


Figure 2. Illustration of the MOSs distribution. HA, AC, and OV quality represent human appearance, action continuity, and overall video, respectively. These abbreviations are used consistently throughout the paper.

point out that current video generation models still struggle with generating realistic human characteristics and actions, which emphasizes the need for quality assessment study in human activity AGVs.

**Video Quality Assessment** studies can be divided into two categories: knowledge-driven methods and data-driven methods. Knowledge-driven BVQA methods leverage prior knowledge to extract quality features (*e.g.*, natural scenes statistics features) for quality regression, such as TLVQM [38], VIDEVAL [77], RAPIQUE [78], etc. In contrast, data-driven BVQA methods automatically learn the quality-aware features by training a carefully designed deep neural network (DNN) in a learning-based manner. Popular data-driven methods generally 1) use a 2D network to extract key frame features and a 3D network to capture motion features from video chunks, as seen in models like BVQA [41], SimpleVQA [71], PatchVQA [96], MinimalisticVQA [73], etc., or 2) employ a 3D network directly to extract video-level features from video chunks, such as FastVQA [87]. The 2D and 3D backbones can be pre-trained on other computer vision tasks [24, 95] or fine-tuned on VQA datasets in an end-to-end manner. Since current VQA research primarily focuses on natural videos, these methods often show limited performance when assessing the quality of AGVs [52].

**AGV Quality Assessment** has been explored in several studies [33, 39, 54]. For instance, FETV [53] benchmarks five T2V models based on static quality, temporal quality, overall alignment, and fine-grained alignment. EvalCrafter [54] evaluates 17 objective metrics, including visual quality, text-video alignment, motion quality, and temporal consistency, on a subjectively-rated AGV dataset. It also proposes a combined metric that leads to improved performance. VBench [33] introduces 16 additional dimensional metrics to evaluate the performance of T2V models. Moreover, [39] constructs the T2VQA-DB, a large-scale text-to-video quality assessment dataset containing 10,000 videos, and develops the T2VQA metric, which focuses on the overall quality of AGVs. Despite these advancements, no specific metric has been developed to evaluate the quality of

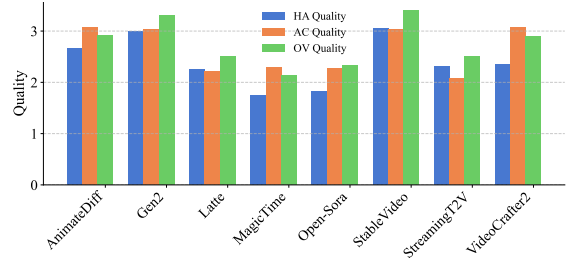


Figure 3. The MOS comparison for 8 T2V models.

human activity AGVs.

### 3. Human-AGVQA Dataset

#### 3.1. Human activity AGVs Collection

**Text Prompts Selection.** Text prompts describe the video content generated by T2V models. To comprehensively analyze the quality assessment problem of human activity AGVs, the selected text prompts in our dataset should cover a wide range of real-world human activities. Therefore, we classify the properties of these words into *ages*, *genders*, *ethnicity*, *occupations*, *scenes*, *emotion*, *appearance*, and *activities* categories and further divide each category into 44 subcategories that frequently occur in daily human life. We then randomly select one subcategory (*e.g.*, *sports*) from the *activity* category, one subcategory (*e.g.*, *outdoor*) from the *scene* category, and two or three subcategories from human appearance-based categories (*e.g.*, *athlete* from the *occupation* category and *male* from the *gender* category). These keywords are combined into a text prompt using GPT-4 [61] with a prompt:

# Please construct a complete sentence based on the following four concepts: “sports”, “outdoor”, “athlete”, and “male”. Note that the specific words “sports”, “outdoor”, “athlete”, and “male” are not required to appear in the sentence, but the sentence should clearly convey the ideas related to these four categories. #.

We also use GPT-4 to evaluate the prompt’s validity, rejecting any that are deemed unreasonable. Using this method, we generate 400 distinct text prompts describing various human activities. The specific subcategories along with their proportions are listed in the supplementary material.

**T2V Models Selection.** We select eight state-of-the-art (SOTA) T2V models, including Gen-2 [16], StableVideo [1], StreamingT2V [26], Video Crafter2 [9], MagicTime [98], Open Sora [40], Latte [55], and Animatediff [22], to generate the video for each prompt. We summarize the detailed information about these T2V models in the supplementary material.

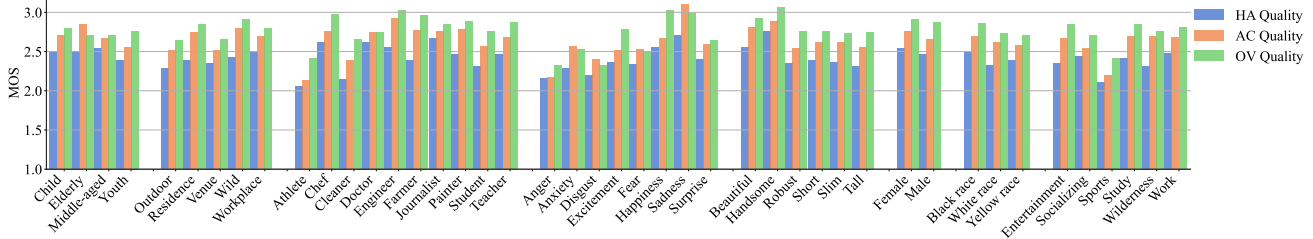


Figure 4. The MOS comparison for 8 text categories and their 44 subcategories.

In summary, a total of 3,200 videos were generated by 8 SOTA T2V models using 400 diverse text prompts in the *Human-AGVQA* dataset.

### 3.2. Quality Assessment Dimensions

We evaluate the quality of human activity AGVs from two perspectives:

**Visual Quality Scoring.** We assess the quality of AGVs from three key dimensions: *human appearance quality*, *action continuity quality*, and *overall video quality*. Specifically, human appearance quality assesses whether the human bodies in the video are complete, semantically correct, and aligned with the prompt description. Action continuity quality focuses on the coherence of the person’s movements, the temporal consistency of limb actions, and whether the actions adhere to the laws of physical motion. Overall video quality evaluates the holistic video quality, including human appearance quality, action continuity quality, as well as background content quality. Participants rate each dimension on a scale from 1 to 5, where 1 represents the lowest quality and 5 represents the highest.

**Semantic Distortion Identification.** Most quality metrics only provide a specific numerical value to quantify video quality, and cannot indicate which parts of the video are distorted or need further enhancement or optimization. This limitation restricts their applicability in quality artifact analysis and fine-grained video quality optimization. To address this, we label the semantic distorted human body parts in AGVs, providing a detailed explanation of quality scores. Specifically, we first annotate whether five body parts (face, arms<sup>1</sup>, torso, legs, feet) are present in AGVs. Then, for each detected body part, we label whether it contains semantic artifacts. Finally, we provide 10 binary labels per AGV for semantic distortion identification.

### 3.3. Subjective Quality Experiment

A total of 80 subjects participated in the visual quality scoring experiment, with ages ranging from 20 to 30 years. The group included 46 males and 34 females. Given that the semantic artifact identification task is less complex than the

<sup>1</sup>Here, the arms include the hands.

visual quality scoring task, we invited 5 experts in the field of AIGC quality assessment to perform the semantic artifact identification. 3,200 videos were divided into eight groups, each containing 400 videos that covered all 400 prompts, and each video was rated by 10 subjects, and labeled by 5 experts. In total, there are 96,000 opinion scores and 160,000 binary labels in the *Human-AGVQA* dataset. Additional details on the subjective experimental settings can be found in the supplemental material.

### 3.4. Data Processing and Analysis

For the quality scoring task, we follow the recommended method in [2] to process the raw subjective ratings into the mean opinion scores (MOSs). For the distortion identification task, we use a voting method to determine body presence and body distortion. The label with the most votes is selected as the final result. The details about data processing and inter-subject consistency are shown in supplementary material.

#### 3.4.1. MOS Distribution Analysis

Figure 2 shows the MOS distributions for the three quality dimensions, which follow a Gaussian distribution. This indicates that medium-quality AGVs outnumber both high- and low-quality AGVs. This suggests that the quality of human activity AGVs still needs improvement to meet visual quality standards. The average MOS for overall video quality is slightly higher than that of action continuity quality, and both are significantly higher than that of human appearance quality. This highlights that generating high-quality realistic humans remains a challenge for current T2V models, underscoring the importance of our study.

#### 3.4.2. MOS Analysis for T2V Models

We calculate the average MOSs of eight T2V models across three quality dimensions to assess their strengths and weaknesses in generating human activity videos. The results are shown in Figure 3. Gen-2 and StableVideo demonstrate superior performance compared to the other T2V models, especially in human appearance quality and overall video quality. Notably, both Gen-2 and StableVideo are commercial T2V tools, indicating that the gener-

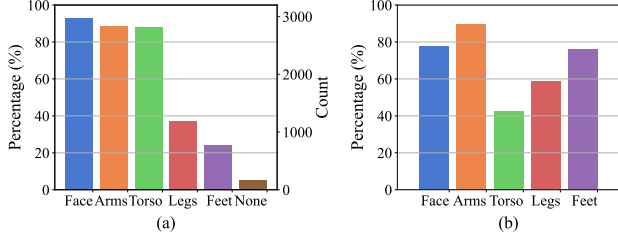


Figure 5. The percentage of AGVs that contain human body parts (a) and the percentage of these body parts exhibit semantic distortions (b).

ation quality of commercial algorithms continues to surpass that of academic open-source models. AnimateDiff and VideoCrafter2 show similar performance to Gen-2 and StableVideo in terms of action continuity quality, highlighting their temporal consistency modeling capabilities.

### 3.4.3. MOS Analysis for Text Prompts

Figure 4 shows the average MOS for 8 text prompt categories and their 44 subcategories. Firstly, for the categories related to human attributes such as age, gender, and race, there is no significant difference in the quality scores among their subcategories, indicating that *the evaluated T2V models do not show bias toward human-related attributes*. Secondly, video quality is generally lower in scenarios involving significant or frequent human movement, such as *outdoor* in the scene category, *athletes* and *cleaners* in the occupation category, and *sports* in the activity category. *This may be because frequent body movements cause the degradation of human appearance*. Thirdly, for the emotion category, simpler emotions such as *sadness* and *happiness* receive relatively high scores, whereas more complex emotions like *anger*, *disgust*, and *anxiety* are not as well-represented, *suggesting that current T2V models continue to face challenges in accurately understanding and representing complex emotions*. Regarding the appearance category, *handsome* and *beautiful* yield satisfactory results. That may be that *the prompts like handsome and beautiful will make the generation model generate high-quality humans*.

### 3.4.4. Semantic Distortion Identification

We counted all body parts appearing in the 3,200 AGVs of the *Human-AGVQA* dataset and the distortions observed for each body part, as shown in Figure 5.

In Figure 5(a), we observe that the face, arms, and torso account for the largest proportions, while the legs and feet are significantly less than three parts. Notably, a small portion of the videos lack any visible body parts, indicating that some T2V models struggle to comprehend the text prompts and generate the corresponding human figures. In Figure 5(b), it is evident that the torso exhibits the fewest

distortions among the five body parts, whereas the face, arms, and legs show more pronounced distortions. This suggests that current T2V models face significant challenges in generating complete and realistic body parts. The performance analysis of T2V models for distortion identification of human bodies can be found in the supplemental material.

## 4. Proposed Model

As illustrated in Figure 6, the proposed AI-generated human activity video quality (GHVQ) methods consists of four modules: a spatial quality analyzer, an action quality analyzer, a text feature extractor, and a quality regressor, which are detailed as follows:

### 4.1. Spatial Quality Analyzer

Assume a video  $\mathbf{x} = \{\mathbf{x}_i\}_{i=0}^{N-1}$  generated by a text prompt  $p$ , where each frame  $\mathbf{x}_i \in \mathbb{R}^{H \times W \times 3}$  denotes the  $i$ -th frame. Here,  $H$  and  $W$  are the height and width of each frame, and  $N$  is the total number of frames. Given the substantial spatial redundancy between video frames, we first temporally downsample the video,  $\mathbf{x}$ , into a lower frame rate sequence,  $\mathbf{y} = \{\mathbf{y}_i\}_{i=0}^{N_s-1}$ , where  $\mathbf{y}_i = \mathbf{x}_{\lfloor N/N_s \times i \rfloor}$ , and  $N_s$  denotes the total number of frames used for extracting spatial features.

We extract spatial quality features from two perspectives: human-focused and holistic, to more accurately evaluate the human appearance quality and overall video quality.

#### 4.1.1. Human-focused Quality Feature Extraction

For frame  $\mathbf{y}_i$ , we first apply a human body-part segmentation model [36], to explicitly detect the body-part masks  $M_i$ , where  $M_i \in \mathbb{R}^{C_m \times H \times W}$  represents five segmentation masks corresponding to the face, arms, torso, legs, feet. Then, we design a shallow hourglass network [60] to extract the high-resolution feature maps  $F_{h,i}$  that preserve the resolution of human appearance while capturing rich low-level features. Here,  $F_{h,i} \in \mathbb{R}^{C_h \times H \times W}$ , with  $C_h$  representing the number of channels of  $F_{h,i}$ .

To focus on features specific to human body regions, we multiply the feature maps  $F_{h,i}$  with the body masks  $M_i$  along the channel dimensions to derive the human body-aware feature maps  $F_{\text{body},i}$ :

$$F_{\text{body},i} = F_{h,i} \cdot M_i, \quad (1)$$

where  $F_{\text{body},i} \in \mathbb{R}^{C_m \times C_b \times H \times W}$ . Next, we develop two modules—the inner-body distortion analysis module (Inner-body DAM) and the cross-body distortion analysis module (Cross-body DAM)—to further extract human-focused quality features at the individual body part level and the body part interaction level, respectively.

**Inner-body DAM.** The inner-body DAM module is designed to capture the quality features related to each individual body part region. This allows the module to analyze

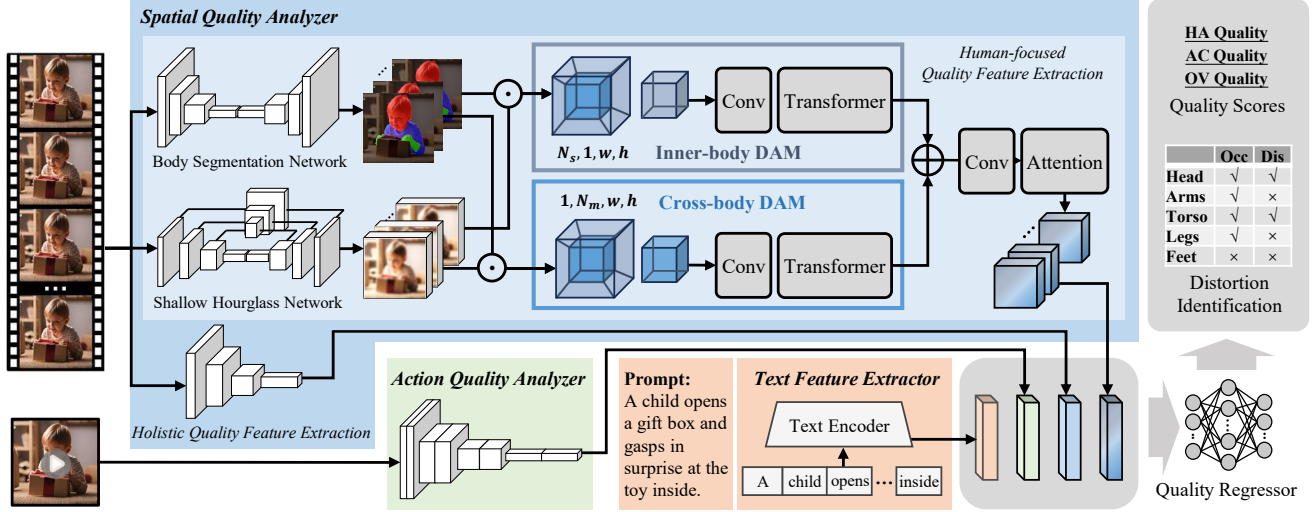


Figure 6. The GHVQ framework comprises four essential modules: a spatial quality analyzer for extracting human-focused and holistic quality features, an action quality analyzer for capturing temporal continuity of the body movement, a text feature extractor for identifying video content that needs to be generated by text prompts, and a quality regressor for mapping these quality-aware features to multi-dimensional quality scores and semantic distortion labels.

each body part separately, helping to assess whether these body parts are presented in the video and which body parts exhibit quality issues. To achieve this, we aggregate the feature maps  $F_{\text{body},i}$  across the channel dimension  $C_h$ :

$$F_{\text{inner},i} = \sum_{j=0}^{C_h-1} F_{\text{body},i}[j, :, :, :], \quad (2)$$

where  $F_{\text{inner},i} \in \mathbb{R}^{C_m \times H \times W}$  contains  $C_m$  feature maps, each focusing on quality analysis for one of the  $C_m$  body parts.

**Cross-body DAM.** In contrast, the cross-body DAM module focuses on capturing interactive relationships between the body parts. Since a complete human action involves the coordinated movement of multiple body parts, jointly considering these interactions can better represent the quality of the human action. To achieve this, we aggregate the feature maps  $F_{\text{body},i}$  across the channel dimension  $C_m$ :

$$F_{\text{cross},i} = \sum_{j=0}^{C_m-1} F_{\text{body},i}[j, :, :, :], \quad (3)$$

where  $F_{\text{cross},i} \in \mathbb{R}^{C_s \times H \times W}$  contains  $C_s$  feature maps focused on the quality analysis of all body parts.

**Feature Refinement and Fusion.** For  $F_{\text{inner},i}$  and  $F_{\text{cross},i}$ , we apply a CNN followed by a Transformer encoder [23] to further refine the inner-body and cross-body features:

$$\begin{aligned} F'_{\text{inner},i} &= \text{Transformer}(\text{Conv}(F_{\text{inner},i})), \\ F'_{\text{cross},i} &= \text{Transformer}(\text{Conv}(F_{\text{cross},i})), \end{aligned} \quad (4)$$

where Transformer denotes the Transformer encoder, and the Conv represents a two-layer CNN. Finally, we concatenate them and then apply a CNN layer followed by a self-attention layer [66] to derive the human-focused quality features:

$$F_{\text{bq},i} = \text{Attention}(\text{Conv}([F'_{\text{inner},i}, F'_{\text{cross},i}])), \quad (5)$$

where Attention denotes the self-attention operator and  $F_{\text{bq},i}$  is the human-focused quality features.

#### 4.1.2. Holistic Quality Feature Extraction

To extract quality-aware features of the entire frame, we pre-train a ViT [15] model on Pick-a-Pic [37], a large-scale text-to-image (T2I) quality assessment dataset, to learn the quality-aware feature representation for AIGC images. Then, for frame  $y_i$ , we employ the pre-trained ViT [15] as the feature extractor to compute the holistic quality features:

$$F_{\text{hq},i} = \text{ViT}(y_i). \quad (6)$$

Finally, we aggregate the human-focused features and the holistic quality features as the spatial quality features, then average them across all sampled frames:

$$\begin{aligned} F_{\text{sq},i} &= [F_{\text{bq},i}, F_{\text{hq},i}], \\ F_{\text{sq}} &= \sum_{i=0}^{N_s-1} F_{\text{sq},i}, \end{aligned} \quad (7)$$

where  $F_{\text{sq},i}$  and  $F_{\text{sq}}$  represent the spatial quality features of frame  $y_i$  and video sequence  $y$ .

Table 1. The performance comparison of existing IQA-based, AQA-based, and VQA-based metrics with our proposed GHVQ metrics on the *Human-AGVQA* dataset. NSC refers to natural scene content.

Quality Dimension	Methods	Pre-training / Initialization	Model Type	Zero-shot		Fine-tuning	
				SRCC	PLCC	SRCC	PLCC
Human Appearance	NIQE (ISPL, 2012) [58]	NA ( <i>handcraft</i> )	NSC	0.234	0.273	0.564	0.583
	BRISQUE (TIP, 2012) [57]	NA ( <i>handcraft</i> )	NSC	0.261	0.314	0.593	0.629
	HyperIQA (CVPR, 2020) [68]	TID2013 [63]	NSC	0.314	0.339	0.684	0.705
	UNIQUE (TIP, 2021) [101]	KonIQ-10K [32]	NSC	0.243	0.280	0.671	0.695
	MUSIQ (ICCV, 2021) [34]	KonIQ-10K [32]	NSC	0.229	0.262	0.584	0.609
	StairIQA (JSTSP, 2023) [72]	KonIQ-10K [32]	NSC	0.334	0.393	0.665	0.671
	CLIP-IQA (AAAI, 2023) [81]	KonIQ-10K [32]	NSC	0.329	0.368	0.672	0.683
	LIQE (CVPR, 2023) [102]	KonIQ-10k [32]	NSC	0.285	0.332	0.641	0.664
	MA-AGIQA (ACMMM, 2024) [84]	AGIQA-3k [43]	AIGC	0.377	0.380	<u>0.728</u>	<u>0.735</u>
	Q-Align (ICML, 2024) [89]	<i>fused</i> [32], [17], [96], [21]	NSC	0.364	0.419	—	—
GHVQ ( <i>proposed</i> )	—	AIGC	—	—	<b>0.812</b>	<b>0.821</b>	
Action Continuity	ACTION-NET (ACMMM, 2020) [99]	Kinetics [6]	NSC	0.197	0.221	0.541	0.551
	USDL (CVPR, 2020) [74]	Kinetics [6]	NSC	0.207	0.260	0.583	0.582
	CoRe (ICCV, 2021) [97]	Kinetics [6]	NSC	0.179	0.213	0.560	0.561
	TSA (CVPR, 2022) [92]	Kinetics [6]	NSC	0.202	0.258	<u>0.607</u>	<u>0.611</u>
	Motion Smoothness (CVPR, 2024) [33]	AMT [48]	AIGC	0.249	0.30	—	—
	Temporal Flickering (CVPR, 2024) [33]	RAFT [75]	AIGC	0.109	0.238	—	—
	Action-Score (CVPR, 2024) [54]	VideoMAE V2 [82]	AIGC	0.208	0.284	—	—
	Flow-Score (CVPR, 2024) [54]	RAFT [75]	AIGC	0.153	0.255	—	—
GHVQ ( <i>proposed</i> )	—	AIGC	—	—	<b>0.788</b>	<b>0.792</b>	
Overall Video	TLVQM (TIP, 2019) [38]	NA ( <i>handcraft</i> )	NSC	0.275	0.314	0.613	0.624
	RAPIQUE (JSP, 2021) [78]	NA ( <i>handcraft</i> )	NSC	0.313	0.351	0.632	0.648
	VIDEAL (TIP, 2021) [77]	NA ( <i>handcraft</i> )	NSC	0.338	0.357	0.638	0.651
	PatchVQ (CVPR, 2021) [96]	LSVQ [96]	NSC	0.378	0.404	0.667	0.703
	SimpleVQA (ACMMM, 2022) [71]	LSVQ [96]	NSC	0.368	0.380	0.695	0.709
	FastVQA (ECCV, 2023) [87]	LSVQ [96]	NSC	0.385	0.408	0.708	0.733
	DOVER (ICCV, 2023) [88]	DIVIDE [88]	NSC	0.315	0.337	0.713	0.736
	T2VQA (ACMMM, 2024) [39]	T2VQA [39]	AIGC	0.357	0.364	<u>0.751</u>	<u>0.754</u>
	UGVQ (Arxiv, 2024) [103]	LGVQ [103]	AIGC	0.349	0.358	0.748	<u>0.757</u>
	EvalCrafter (CVPR, 2024) [54]	DIVIDE [88]	NSC	0.328	0.341	—	—
	Q-Align (ICML, 2024) [89]	<i>fused</i> [32], [17], [96], [21]	AIGC	0.427	0.485	—	—
GHVQ ( <i>proposed</i> )	—	AIGC	—	—	<b>0.780</b>	<b>0.788</b>	

## 4.2. Action Quality Analyzer

The action quality analyzer is designed to quantify temporal continuity of videos, serving as a complement to the spatial quality analyzer in assessing comprehensively the quality of AGVs. To address this, we utilize an action recognition model, as the action quality analyzer to capture the temporal continuity of human body movement. Since action recognition models are trained on large-scale, authentic-captured human action datasets, such as the Kinetics series [6], they can effectively extract motion representations of human bodies. Moreover, previous VQA studies [71] have also demonstrated that these features are useful for video quality evaluation. Specifically, for video  $x$  and the action recognition network SlowFast [19], we calculate the action quality features  $F_{aq}$  using all frames in  $x$ .

## 4.3. Text Feature Extractor

Since the purpose of T2V models is to generate video content that aligns with the text prompt, it is necessary to measure the alignment between the video content and the text prompt. Following most T2I and T2V alignment evaluation studies [33, 84], we utilize the text encoder of CLIP [37] to extract semantic features  $F_{tq}$  of the text prompt  $p$ .

## 4.4. Quality Regressor

The quality regressor is used to assess the three quality scores and determine whether human bodies are present and if there exist semantic distortions. So, we first integrate the spatial quality features, the action quality features, and the text features into the final quality-aware features  $F_q$ :

$$F_q = [F_{sq}, F_{aq}, F_{tq}]. \quad (8)$$

Then,  $F_q$  are fed into two multi-layer perceptron (MLP) to produce the quality scores  $\hat{q}$  and distortion labels  $\hat{b}$ .

The loss function consists of the mean absolute error (MAE) loss, rank loss [39], and binary cross-entropy loss. The MAE loss, and rank loss are used to optimize the quality scoring task, and the binary cross-entropy loss is used to optimize the distortion identification task.

## 5. Experiments

### 5.1. Experiment Settings

**Compared Quality Metrics.** Since no specific metrics have been designed to evaluate human appearance quality, we compared 10 IQA models to assess the quality of video frames as a proxy for human appearance. For action continuity quality and overall video quality, we select 8

Table 2. The accuracy of video LMM models in identifying the occurrences and distortions of body parts in the *Human-AGVQA* dataset.

Models	Occurrences / Distortions					
	Face	Arms	Torso	Legs	Feet	Avg
LLaMAVID (7B) [47]	91.9 / 56.6	82.9 / 62.1	81.8 / 46.5	37.2 / 30.7	25.1 / 41.5	63.8 / 47.7
VideoChatGPT (7B) [56]	73.9 / 71.7	79.7 / 76.2	75.2 / 37.6	38.8 / 23.0	29.2 / 19.4	59.4 / 45.6
VideoLLaMA2 (7B) [11]	22.5 / 24.9	14.1 / 14.9	41.2 / 61.2	61.9 / 75.8	70.4 / 78.3	42.2 / 51.0
VILA1.5 (7B) [51]	22.4 / 36.6	20.1 / 22.5	16.5 / 60.7	60.8 / 74.7	71.3 / 76.8	38.2 / 54.3
NeXT-Video (7B) [44]	62.5 / 37.6	56.8 / 22.5	78.6 / 60.9	58.2 / 75.0	65.3 / 77.6	64.3 / 54.7
OneVison (7B) [42]	61.9 / 29.8	71.9 / 19.8	64.6 / 62.2	52.2 / 77.0	67.2 / 80.3	63.6 / 53.8
Qwen2-VL (7B) [83]	63.1 / 44.3	57.9 / 25.7	71.0 / 60.4	62.6 / 76.1	74.1 / 79.9	70.3 / 57.3
GPT-4o [61]	92.4 / 29.7	89.7 / 19.3	85.1 / 61.6	62.1 / 77.4	76.1 / 80.1	80.0 / 53.6
GPT-4o-mini [61]	90.6 / 28.4	86.5 / 20.1	82.7 / 60.4	62.6 / 75.3	74.0 / 77.3	78.6 / 52.3
GHVQ (proposed)	92.6 / 72.3	87.1 / 80.6	87.1 / 63.4	63.5 / 78.1	77.2 / 81.5	81.5 / 75.2

action quality assessment (AQA) and 11 VQA methods as comparison respectively. For body parts detection and their distortion identification, there are also no specific metrics, we benchmark 9 general video large multi-modality (LMM) model for this task. A detailed introduction to these methods can be found in the supplemental material.

**Dataset Splits.** We split the *Human-AGVQA* dataset into 70% for training, 10% for validation, and 20% for test. For video quality scoring, the compared metrics are evaluated on the test set using two approaches: zero-shot testing and fine-tuning testing. For body parts detection and distortion identification, we directly test zero-shot performance of compared LMMs.

**Evaluation Criteria.** We use PLCC and SRCC to evaluate the performance of the test metrics. Additionally, we use classification accuracy to assess the performance of body part detection and distortion identification.

Other experimental settings including the training details of GHVQ can be found in the supplemental material.

## 5.2. Performance Comparison

### 5.2.1. Quality Scoring Task

**Human Appearance Quality.** We observe that all compared IQA methods perform poorly in evaluating human appearance quality in the zero-shot setting, which highlights that distortions in human appearance in AGVs represent entirely new artifacts that existing metrics cannot handle. Fine-tuning on the *Human-AGVQA* dataset improves the performance of data-driven methods, but their results remain suboptimal. This may be because these methods focus on learning feature representations from global images, rather than human-focused regions. The proposed GHVQ achieves the best performance, outperforming the second-best method by 0.812 and 0.821 in terms of SRCC and PLCC, demonstrating the effectiveness of its design for extracting human appearance-focused features.

**Action Continuity Quality.** Similar to human appearance quality, the compared AVA methods and temporal metrics

Table 3. Ablation study results for different modules across quality metrics. SQA, AQA, and TFE refer to the spatial quality analyzer, action quality analyzer, and text feature extractor, respectively. The results for the three quality scores are reported using SRCC/PLCC, while distortion identification is presented in terms of occurrence and distortion accuracy.

SQA	AQA	TFE	HA Quality	AC Quality	OV Quality	Distortion Identification
	✓	✓	0.633 / 0.638	0.617 / 0.631	0.724 / 0.733	0.575 / 0.512
✓		✓	0.767 / 0.770	0.747 / 0.748	0.728 / 0.740	0.753 / 0.704
✓	✓		0.781 / 0.789	0.754 / 0.765	0.773 / 0.776	0.802 / 0.736
✓	✓	✓	0.812 / 0.821	0.788 / 0.792	0.780 / 0.788	0.815 / 0.752

of AIGC VQA methods show a very low correlation in assessing action continuity quality. This is because AVA methods are typically designed to quantify the completeness of professional sports performances, while the temporal metrics in AIGC VQA methods rely on handcrafted motion descriptors that do not capture semantic content, such as those involving individuals. In the fine-tuning results, GHVQ outperforms the re-trained AVA methods, surpassing the second-best method by 0.788 and 0.792 in terms of SRCC and PLCC, demonstrating that the proposed model architecture is better suited to measure action continuity quality.

**Overall Video Quality.** The performance of VQA metrics in assessing overall video quality is slightly superior to that of other metrics for human appearance and action continuity quality. Generally, we find that AIGC-based VQA methods outperform general data-driven VQA methods, and both of these are more effective than knowledge-driven VQA methods. Similarly, re-training these methods leads to significant improvements. Since GHVQ comprehensively extracts human-focused, action continuity, and holistic frame quality features, the proposed GHVQ outperforms existing VQA methods, improving performance by 0.780 and 0.788 in terms of SRCC and PLCC.

### 5.2.2. Body Presence and Distortion Identifying Task

Identifying the presence and distortions of human body parts is a novel task, and we benchmark the performance of video LMM models for this task in Table 2. As for LMMS, GPT-4 series perform best in terms of detecting the presence of body parts, while Qwen2-VL achieve the highest accuracy in identifying whether body parts exhibit semantic distortions. We observe that that identifying distortions in arms is the most challenging, followed by facial distortions while detecting distortions in legs and feet is relatively easier. This aligns with the inherent complexity of structures like faces and arms (particularly hands). Overall, our GHVQ model outperforms in both presence detection and distortion identification tasks, improving accuracy by 1.8% and 28.3%, respectively.



### 5.3. Ablation Study

We conducted an ablation study to validate the effectiveness of the spatial quality analyzer, action quality analyzer, and text feature extractor. The experimental results are shown in Table 3. We observe that the performance across all three quality dimensions and distortion identification degrades the most when the spatial quality analyzer is removed, highlighting the importance of extracting human-focused and AIGC-aware quality features. The action quality analyzer is less crucial than the spatial quality analyzer, possibly because the pre-trained action recognition model is less sensitive to motion in AGVs. The text feature extractor has the least impact compared to the spatial and action quality analyzers, as it only captures video content based on text prompts and does not directly engage with AGVs. In summary, the combination of all three modules achieves the highest performance across all quality dimensions.

## 6. Conclusion

In this paper, we present an in-depth quality assessment study on human activity AGVs, which includes the construction of the large-scale human activity AGV dataset Human-AGVQA and the development of the objective quality metric GHVQ for human activity AGVs. The diversity of human activities and the richness of quality labels in Human-AGVQA make it well-suited for developing and validating quality metrics for human activity AGVs. The GHVQ metric has demonstrated strong performance in assessing these videos, making it a valuable tool for T2V studies to measure progress in generating human activity content. We hope these contributions will promote the development and application of T2V models.

## References

- [1] Stablevideo. 1, 2, 3, 7
- [2] Methodology for the subjective assessment of the quality of television pictures. *International Telecommunication Union*, 2002. 4
- [3] Jake Bruce, Michael Dennis, Ashley Edwards, Jack Parker-Holder, Yuge Shi, Edward Hughes, Matthew Lai, Aditi Mavalankar, Richie Steigerwald, Chris Apps, et al. Gennie: Generative interactive environments. *arXiv preprint arXiv:2402.15391*, 2024. 2
- [4] Zhe Cao, Tomas Simon, Shih-En Wei, and Yaser Sheikh. Realtime multi-person 2d pose estimation using part affinity fields. In *Proceedings of the IEEE Conference on Computer Vision and Pattern Recognition (CVPR)*, pages 7291–7299, 2017. 11
- [5] Joao Carreira and Andrew Zisserman. Quo vadis, action recognition? a new model and the kinetics dataset. In *Proceedings of the IEEE conference on Computer Vision and Pattern Recognition (CVPR)*, pages 6299–6308, 2017. 11
- [6] Joao Carreira and Andrew Zisserman. Quo vadis, action recognition? a new model and the kinetics dataset. In *proceedings of the IEEE Conference on Computer Vision and Pattern Recognition*, pages 6299–6308, 2017. 7
- [7] Haoxin Chen, Menghan Xia, Yingqing He, Yong Zhang, Xiaodong Cun, Shaoshu Yang, Jinbo Xing, Yaofang Liu, Qifeng Chen, Xintao Wang, et al. Videocrafter1: Open diffusion models for high-quality video generation. *arXiv preprint arXiv:2310.19512*, 2023. 2
- [8] Haoxin Chen, Yong Zhang, Xiaodong Cun, Menghan Xia, Xintao Wang, Chao Weng, and Ying Shan. Videocrafter2: Overcoming data limitations for high-quality video diffusion models. *arXiv preprint arXiv:2401.09047*, 2024. 2
- [9] Haoxin Chen, Yong Zhang, Xiaodong Cun, Menghan Xia, Xintao Wang, Chao Weng, and Ying Shan. Videocrafter2: Overcoming data limitations for high-quality video diffusion models. *arXiv*, 2024. 1, 3, 2, 7
- [10] Liang-Chieh Chen, Yukun Zhu, George Papandreou, Florian Schroff, and Hartwig Adam. Encoder-decoder with atrous separable convolution for semantic image segmentation. In *Proceedings of the European Conference on Computer Vision (ECCV)*, pages 801–818, 2018. 11
- [11] Zesen Cheng, Sicong Leng, Hang Zhang, Yifei Xin, Xin Li, Guanzheng Chen, Yongxin Zhu, Wenqi Zhang, Ziyang Luo, Deli Zhao, et al. Videollama 2: Advancing spatial-temporal modeling and audio understanding in video-llms. *arXiv preprint arXiv:2406.07476*, 2024. 8
- [12] Mehdi Cherti, Romain Beaumont, Ross Wightman, Mitchell Wortsman, Gabriel Ilharco, Cade Gordon, Christoph Schuhmann, Ludwig Schmidt, and Jenia Jitsev. Reproducible scaling laws for contrastive language-image learning. In *Proceedings of the IEEE/CVF Conference on Computer Vision and Pattern Recognition*, pages 2818–2829, 2023. 11
- [13] Joseph Cho, Fachrina Dewi Puspitasari, Sheng Zheng, Jingyao Zheng, Lik-Hang Lee, Tae-Ho Kim, Choong Seon Hong, and Chaoning Zhang. Sora as an agi world model? a complete survey on text-to-video generation. *arXiv preprint arXiv:2403.05131*, 2024. 2
- [14] Kangle Deng, Tianyi Fei, Xin Huang, and Yuxin Peng. Irgan: Introspective recurrent convolutional gan for text-to-video generation. In *IJCAI*, pages 2216–2222, 2019. 2
- [15] Alexey Dosovitskiy, Lucas Beyer, Alexander Kolesnikov, Dirk Weissenborn, Xiaohua Zhai, Thomas Unterthiner, Mostafa Dehghani, Matthias Minderer, Georg Heigold, Sylvain Gelly, Jakob Uszkoreit, and Neil Houlsby. An image is worth 16x16 words: Transformers for image recognition at scale, 2021. 6
- [16] Patrick Esser, Johnathan Chiu, Parmida Atighehchian, Jonathan Granskog, and Anastasis Germanidis. Structure and content-guided video synthesis with diffusion models. In *Proceedings of the IEEE/CVF International Conference on Computer Vision (ICCV)*, pages 7346–7356, 2023. 2, 3, 7
- [17] Yuming Fang, Hanwei Zhu, Yan Zeng, Kede Ma, and Zhou Wang. Perceptual quality assessment of smartphone photography. In *Proceedings of the IEEE/CVF conference on*

- computer vision and pattern recognition*, pages 3677–3686, 2020. 7
- [18] Christoph Feichtenhofer. X3d: Expanding architectures for efficient video recognition. In *Proceedings of the IEEE/CVF Conference on Computer Vision and Pattern Recognition (CVPR)*, pages 2036–2045, 2020. 11
- [19] Christoph Feichtenhofer, Haoqi Fan, Jitendra Malik, and Kaiming He. Slowfast networks for video recognition. In *2019 IEEE/CVF International Conference on Computer Vision (ICCV)*, pages 6201–6210, 2019. 7, 11
- [20] Songwei Ge, Thomas Hayes, Harry Yang, Xi Yin, Guan Pang, David Jacobs, Jia-Bin Huang, and Devi Parikh. Long video generation with time-agnostic vqgan and time-sensitive transformer. In *European Conference on Computer Vision*, pages 102–118. Springer, 2022. 2
- [21] Chunhui Gu, Chen Sun, David A Ross, Carl Vondrick, Caroline Pantofaru, Yeqing Li, Sudheendra Vijayanarasimhan, George Toderici, Susanna Ricco, Rahul Sukthankar, et al. Ava: A video dataset of spatio-temporally localized atomic visual actions. In *Proceedings of the IEEE conference on computer vision and pattern recognition*, pages 6047–6056, 2018. 7
- [22] Yuwei Guo, Ceyuan Yang, Anyi Rao, Zhengyang Liang, Yaohui Wang, Yu Qiao, Maneesh Agrawala, Dahua Lin, and Bo Dai. Animatediff: Animate your personalized text-to-image diffusion models without specific tuning. *International Conference on Learning Representations*, 2024. 3, 2, 7
- [23] Kai Han, An Xiao, Enhua Wu, Jianyuan Guo, Chunjing Xu, and Yunhe Wang. Transformer in transformer. *Advances in neural information processing systems*, 34:15908–15919, 2021. 6
- [24] Kaiming He, Xiangyu Zhang, Shaoqing Ren, and Jian Sun. Deep residual learning for image recognition. In *Proceedings of the IEEE conference on computer vision and pattern recognition*, pages 770–778, 2016. 3
- [25] Yingqing He, Tianyu Yang, Yong Zhang, Ying Shan, and Qifeng Chen. Latent video diffusion models for high-fidelity long video generation. *arXiv preprint arXiv:2211.13221*, 2022. 2
- [26] Roberto Henschel, Levon Khachatryan, Daniil Hayrapetyan, Hayk Poghosyan, Vahram Tadevosyan, Zhangyang Wang, Shant Navasardyan, and Humphrey Shi. Streamingt2v: Consistent, dynamic, and extendable long video generation from text. *arXiv preprint arXiv:2403.14773*, 2024. 3, 2, 7
- [27] Jack Hessel, Ari Holtzman, Maxwell Forbes, Ronan Le Bras, and Yejin Choi. Clipscore: A reference-free evaluation metric for image captioning. In *Proceedings of the 2021 Conference on Empirical Methods in Natural Language Processing (EMNLP)*, pages 7514–7528, 2021. 11
- [28] Martin Heusel, Hubert Ramsauer, Thomas Unterthiner, Bernhard Nessler, and Sepp Hochreiter. Gans trained by a two time-scale update rule converge to a local nash equilibrium. In *Advances in Neural Information Processing Systems*. Curran Associates, Inc., 2017. 2
- [29] Jonathan Ho, William Chan, Chitwan Saharia, Jay Whang, Ruiqi Gao, Alexey Gritsenko, Diederik P. Kingma, Ben Poole, Mohammad Norouzi, David J. Fleet, and Tim Salimans. Imagen video: High definition video generation with diffusion models, 2022. 2
- [30] Jonathan Ho, Tim Salimans, Alexey Gritsenko, William Chan, Mohammad Norouzi, and David J Fleet. Video diffusion models. *Advances in Neural Information Processing Systems*, 35:8633–8646, 2022. 2
- [31] Wenyi Hong, Ming Ding, Wendi Zheng, Xinghan Liu, and Jie Tang. Cogvideo: Large-scale pretraining for text-to-video generation via transformers. In *The Eleventh International Conference on Learning Representations*, 2022. 2
- [32] Vlad Hosu, Hanhe Lin, Tamas Sziranyi, and Dietmar Saupe. Koniq-10k: An ecologically valid database for deep learning of blind image quality assessment. *IEEE Transactions on Image Processing*, 29:4041–4056, 2020. 7
- [33] Ziqi Huang, Yanan He, Jiashuo Yu, Fan Zhang, Chenyang Si, Yuming Jiang, Yuanhan Zhang, Tianxing Wu, Qingyang Jin, Nattapol Chanpaisit, Yaohui Wang, Xinyuan Chen, Limin Wang, Dahua Lin, Yu Qiao, and Ziwei Liu. VBench: Comprehensive benchmark suite for video generative models. In *Proceedings of the IEEE/CVF Conference on Computer Vision and Pattern Recognition*, 2024. 2, 3, 7, 10
- [34] Junjie Ke, Qifei Wang, Yilin Wang, Peyman Milanfar, and Feng Yang. Musiq: Multi-scale image quality transformer. In *2021 IEEE/CVF International Conference on Computer Vision (ICCV)*, pages 5128–5137, 2021. 7, 9
- [35] Levon Khachatryan, Andranik Movsisyan, Vahram Tadevosyan, Roberto Henschel, Zhangyang Wang, Shant Navasardyan, and Humphrey Shi. Text2video-zero: Text-to-image diffusion models are zero-shot video generators. In *Proceedings of the IEEE/CVF International Conference on Computer Vision*, pages 15954–15964, 2023. 2
- [36] Rawal Khirodkar, Timur Bagautdinov, Julieta Martinez, Su Zhaoen, Austin James, Peter Selednik, Stuart Anderson, and Shunsuke Saito. Sapiens: Foundation for human vision models, 2024. 5, 11
- [37] Yuval Kirstain, Adam Poliak, Uriel Singer, and Omer Levy. Pick-a-pic: An open dataset of user preferences for text-to-image generation. In *Advances in Neural Information Processing Systems*, 2023. 6, 7, 11
- [38] Jari Korhonen. Two-level approach for no-reference consumer video quality assessment. *IEEE Transactions on Image Processing*, 28(12):5923–5938, 2019. 3, 7, 9
- [39] Tengchuan Kou, Xiaohong Liu, Zicheng Zhang, Chunyi Li, Haoning Wu, Xiongkuo Min, Guangtao Zhai, and Ning Liu. Subjective-aligned dataset and metric for text-to-video quality assessment. In *Proceedings of the 32nd ACM International Conference on Multimedia*, pages 7793–7802, 2024. 2, 3, 7, 10
- [40] PKU-Yuan Lab and Tuzhan AI etc. Open-sora-plan, 2024. 3, 2, 7
- [41] Bowen Li, Weixia Zhang, Meng Tian, Guangtao Zhai, and Xianpei Wang. Blindly assess quality of in-the-wild videos via quality-aware pre-training and motion perception. *IEEE Transactions on Circuits and Systems for Video Technology*, 32(9):5944–5958, 2022. 3
- [42] Bo Li, Yuanhan Zhang, Dong Guo, Renrui Zhang, Feng Li, Hao Zhang, Kaichen Zhang, Yanwei Li, Ziwei Liu, and

- Chunyu Li. Llava-onevision: Easy visual task transfer. *arXiv preprint arXiv:2408.03326*, 2024. 8
- [43] Chunyi Li, Zicheng Zhang, Haoning Wu, Wei Sun, Xiongkuo Min, Xiaohong Liu, Guangtao Zhai, and Weisi Lin. Agiqa-3k: An open database for ai-generated image quality assessment. *IEEE Transactions on Circuits and Systems for Video Technology*, pages 1–1, 2023. 7
- [44] Feng Li, Renrui Zhang, Hao Zhang, Yuanhan Zhang, Bo Li, Wei Li, Zejun Ma, and Chunyu Li. Llava-next-interleave: Tackling multi-image, video, and 3d in large multimodal models. *arXiv preprint arXiv:2407.07895*, 2024. 8
- [45] Junnan Li, Dongxu Li, Caiming Xiong, and Steven Hoi. Blip: Bootstrapping language-image pre-training for unified vision-language understanding and generation. In *ICML*, 2022. 11
- [46] Yitong Li, Martin Min, Dinghan Shen, David Carlson, and Lawrence Carin. Video generation from text. In *Proceedings of the AAAI conference on artificial intelligence*, 2018. 2
- [47] Yanwei Li, Chengyao Wang, and Jiaya Jia. Llama-vid: An image is worth 2 tokens in large language models. In *Computer Vision – ECCV 2024*, pages 323–340, Cham, 2025. Springer Nature Switzerland. 8
- [48] Zhen Li, Zuo-Liang Zhu, Ling-Hao Han, Qibin Hou, Chun-Le Guo, and Ming-Ming Cheng. Amt: All-pairs multi-field transforms for efficient frame interpolation. In *Proceedings of the IEEE/CVF Conference on Computer Vision and Pattern Recognition*, pages 9801–9810, 2023. 7
- [49] Jian Liang, Chenfei Wu, Xiaowei Hu, Zhe Gan, Jianfeng Wang, Lijuan Wang, Zicheng Liu, Yuejian Fang, and Nan Duan. Nuwa-infinity: Autoregressive over autoregressive generation for infinite visual synthesis. *Advances in Neural Information Processing Systems*, 35:15420–15432, 2022. 2
- [50] Xiaodan Liang, Ke Gong, Xiaohui Shen, and Liang Lin. Look into person: Joint body parsing & pose estimation network and a new benchmark. In *IEEE Transactions on Pattern Analysis and Machine Intelligence (TPAMI)*, 2018. 11
- [51] Ji Lin, Hongxu Yin, Wei Ping, Pavlo Molchanov, Mohammad Shoybi, and Song Han. Vila: On pre-training for visual language models. In *Proceedings of the IEEE/CVF Conference on Computer Vision and Pattern Recognition (CVPR)*, pages 26689–26699, 2024. 8
- [52] Xiao Liu, Xinhao Xiang, Zizhong Li, Yongheng Wang, Zhuoheng Li, Zhuosheng Liu, Weidi Zhang, Weiqi Ye, and Jiawei Zhang. A survey of ai-generated video evaluation. *arXiv preprint arXiv:2410.19884*, 2024. 3
- [53] Yuanxin Liu, Lei Li, Shuhuai Ren, Rundong Gao, Shicheng Li, Sishuo Chen, Xu Sun, and Lu Hou. Fetv: A benchmark for fine-grained evaluation of open-domain text-to-video generation. *arXiv preprint arXiv: 2311.01813*, 2023. 2, 3
- [54] Yaofang Liu, Xiaodong Cun, Xuebo Liu, Xintao Wang, Yong Zhang, Haoxin Chen, Yang Liu, Tiejong Zeng, Raymond Chan, and Ying Shan. Evalcrafter: Benchmarking and evaluating large video generation models. In *Proceedings of the IEEE/CVF Conference on Computer Vision and Pattern Recognition (CVPR)*, pages 22139–22149, 2024. 2, 3, 7, 10
- [55] Xin Ma, Yaohui Wang, Gengyun Jia, Xinyuan Chen, Ziwei Liu, Yuan-Fang Li, Cunjian Chen, and Yu Qiao. Latte: Latent diffusion transformer for video generation. *arXiv preprint arXiv:2401.03048*, 2024. 3, 2, 7
- [56] Muhammad Maaz, Hanoona Rasheed, Salman Khan, and Fahad Shahbaz Khan. Video-chatgpt: Towards detailed video understanding via large vision and language models. *arXiv preprint arXiv:2306.05424*, 2023. 8
- [57] Anish Mittal, Anush Krishna Moorthy, and Alan Conrad Bovik. No-reference image quality assessment in the spatial domain. *IEEE Transactions on image processing*, 21(12): 4695–4708, 2012. 7, 9
- [58] Anish Mittal, Rajiv Soundararajan, and Alan C Bovik. Making a “completely blind” image quality analyzer. *IEEE Signal processing letters*, 20(3):209–212, 2012. 7, 9
- [59] Gaurav Mittal, Tanya Marwah, and Vineeth N Balasubramanian. Sync-draw: Automatic video generation using deep recurrent attentive architectures. In *Proceedings of the 25th ACM international conference on Multimedia*, pages 1096–1104, 2017. 2
- [60] Alejandro Newell, Kaiyu Yang, and Jia Deng. Stacked hourglass networks for human pose estimation, 2016. 5
- [61] OpenAI. Chatgpt (version 4), 2024. 3, 8
- [62] Yingwei Pan, Zhaofan Qiu, Ting Yao, Houqiang Li, and Tao Mei. To create what you tell: Generating videos from captions. In *Proceedings of the 25th ACM international conference on Multimedia*, pages 1789–1798, 2017. 2
- [63] Nikolay Ponomarenko, Lina Jin, Oleg Ieremeiev, Vladimir Lukin, Karen Egiazarian, Jaakko Astola, Benoit Vozel, Kacem Chehdi, Marco Carli, Federica Battisti, et al. Image database tid2013: Peculiarities, results and perspectives. *Signal processing: Image communication*, 30:57–77, 2015. 7
- [64] A. Radford, J. W. Kim, C. Hallacy, A. Ramesh, G. Goh, S. Agarwal, G. Sastry, A. Askell, P. Mishkin, J. Clark, G. Krueger, and I. Sutskever. Learning transferable visual models from natural language supervision. *Proceedings of the 38th International Conference on Machine Learning (ICML)*, 2021. 11
- [65] Tim Salimans, Ian Goodfellow, Wojciech Zaremba, Vicki Cheung, Alec Radford, and Xi Chen. Improved techniques for training gans. *Advances in neural information processing systems*, 29, 2016. 2
- [66] Peter Shaw, Jakob Uszkoreit, and Ashish Vaswani. Self-attention with relative position representations. *arXiv preprint arXiv:1803.02155*, 2018. 6
- [67] Uriel Singer, Adam Polyak, Thomas Hayes, Xi Yin, Jie An, Songyang Zhang, Qiyuan Hu, Harry Yang, Oron Ashual, Oran Gafni, et al. Make-a-video: Text-to-video generation without text-video data. *arXiv preprint arXiv:2209.14792*, 2022. 2
- [68] Shaolin Su, Qingsen Yan, Yu Zhu, Cheng Zhang, Xin Ge, Jinqiu Sun, and Yanning Zhang. Blindly assess image quality in the wild guided by a self-adaptive hyper network. In *Proceedings of the IEEE/CVF Conference on Computer Vision and Pattern Recognition (CVPR)*, 2020. 7, 9

- [69] Ke Sun, Bin Xiao, Dong Liu, and Jingdong Wang. Deep high-resolution representation learning for human pose estimation. In *Proceedings of the IEEE/CVF Conference on Computer Vision and Pattern Recognition (CVPR)*, pages 5693–5703, 2019. 11
- [70] Rui Sun, Yumin Zhang, Tejal Shah, Jiaohao Sun, Shuoying Zhang, Wenqi Li, Haoran Duan, and Bo Wei. From sora what we can see: A survey of text-to-video generation. 2
- [71] Wei Sun, Xiongkuo Min, Wei Lu, and Guangtao Zhai. A deep learning based no-reference quality assessment model for ugc videos. In *Proceedings of the 30th ACM International Conference on Multimedia*, page 856–865, 2022. 3, 7, 9
- [72] Wei Sun, Xiongkuo Min, Danyang Tu, Siwei Ma, and Guangtao Zhai. Blind quality assessment for in-the-wild images via hierarchical feature fusion and iterative mixed database training. *IEEE Journal of Selected Topics in Signal Processing*, 2023. 7, 9
- [73] Wei Sun, Wen Wen, Xiongkuo Min, Long Lan, Guangtao Zhai, and Kede Ma. Analysis of video quality datasets via design of minimalistic video quality models. *IEEE Transactions on Pattern Analysis and Machine Intelligence*, 2024. 3
- [74] Yansong Tang, Zanlin Ni, Jiahuan Zhou, Danyang Zhang, Jiwen Lu, Ying Wu, and Jie Zhou. Uncertainty-aware score distribution learning for action quality assessment. In *Proceedings of the IEEE/CVF Conference on Computer Vision and Pattern Recognition (CVPR)*, 2020. 7, 10
- [75] Zachary Teed and Jia Deng. Raft: Recurrent all-pairs field transforms for optical flow. In *Computer Vision—ECCV 2020: 16th European Conference, Glasgow, UK, August 23–28, 2020, Proceedings, Part II 16*, pages 402–419. Springer, 2020. 7
- [76] Du Tran, Lubomir Bourdev, Rob Fergus, Lorenzo Torresani, and Manohar Paluri. Learning spatiotemporal features with 3d convolutional networks. In *Proceedings of the IEEE International Conference on Computer Vision (ICCV)*, pages 4489–4497, 2015. 11
- [77] Zhengzhong Tu, Yilin Wang, Neil Birkbeck, Balu Adsumilli, and Alan C Bovik. Ugc-vqa: Benchmarking blind video quality assessment for user generated content. *IEEE Transactions on Image Processing*, 30:4449–4464, 2021. 3, 7, 9
- [78] Zhengzhong Tu, Xiangxu Yu, Yilin Wang, Neil Birkbeck, Balu Adsumilli, and Alan C. Bovik. Rapique: Rapid and accurate video quality prediction of user generated content. *IEEE Open Journal of Signal Processing*, 2:425–440, 2021. 3, 7, 9
- [79] Thomas Unterthiner, Sjoerd van Steenkiste, Karol Kurach, Raphael Marinier, Marcin Michalski, and Sylvain Gelly. Towards accurate generative models of video: A new metric challenges, 2019. 2
- [80] Ruben Villegas, Mohammad Babaeizadeh, Pieter-Jan Kindermans, Hernan Moraldo, Han Zhang, Mohammad Taghi Saffar, Santiago Castro, Julius Kunze, and Dumitru Erhan. Phenaki: Variable length video generation from open domain textual descriptions. In *International Conference on Learning Representations*, 2022. 2
- [81] Jianyi Wang, Kelvin C.K. Chan, and Chen Change Loy. Exploring clip for assessing the look and feel of images. *Proceedings of the AAAI Conference on Artificial Intelligence*, 37(2):2555–2563, 2023. 7, 9
- [82] Limin Wang, Bingkun Huang, Zhiyu Zhao, Zhan Tong, Yinan He, Yi Wang, Yali Wang, and Yu Qiao. Videomae v2: Scaling video masked autoencoders with dual masking. In *Proceedings of the IEEE/CVF Conference on Computer Vision and Pattern Recognition*, pages 14549–14560, 2023. 7
- [83] Peng Wang, Shuai Bai, Sinan Tan, Shijie Wang, Zhihao Fan, Jinze Bai, Keqin Chen, Xuejing Liu, Jialin Wang, Wenbin Ge, et al. Qwen2-vl: Enhancing vision-language model’s perception of the world at any resolution. *arXiv preprint arXiv:2409.12191*, 2024. 8
- [84] Puyi Wang, Wei Sun, Zicheng Zhang, Jun Jia, Yanwei Jiang, Zhichao Zhang, Xiongkuo Min, and Guangtao Zhai. Large multi-modality model assisted ai-generated image quality assessment. In *Proceedings of the 32nd ACM International Conference on Multimedia*, pages 7803–7812, 2024. 2, 7, 9
- [85] Yi Wang, Kunchang Li, Yizhuo Li, Yinan He, Bingkun Huang, Zhiyu Zhao, Hongjie Zhang, Jilan Xu, Yi Liu, Zun Wang, Sen Xing, Guo Chen, Junting Pan, Jiashuo Yu, Yali Wang, Limin Wang, and Yu Qiao. Internvideo: General video foundation models via generative and discriminative learning. *arXiv preprint arXiv:2212.03191*, 2022. 11
- [86] Chenfei Wu, Jian Liang, Lei Ji, Fan Yang, Yuejian Fang, Daxin Jiang, and Nan Duan. Nüwa: Visual synthesis pre-training for neural visual world creation. In *European conference on computer vision*, pages 720–736. Springer, 2022. 2
- [87] Haoning Wu, Chaofeng Chen, Jingwen Hou, Liang Liao, Annan Wang, Wenxiu Sun, Qiong Yan, and Weisi Lin. Fastvqa: Efficient end-to-end video quality assessment with fragment sampling. In *Computer Vision – ECCV 2022: 17th European Conference, Tel Aviv, Israel, October 23–27, 2022, Proceedings, Part VI*, page 538–554, Berlin, Heidelberg, 2022. Springer-Verlag. 3, 7, 9
- [88] Haoning Wu, Erli Zhang, Liang Liao, Chaofeng Chen, Jingwen Hou, Annan Wang, Wenxiu Sun, Qiong Yan, and Weisi Lin. Exploring video quality assessment on user generated contents from aesthetic and technical perspectives. In *International Conference on Computer Vision (ICCV)*, 2023. 7, 9
- [89] Haoning Wu, Zicheng Zhang, Weixia Zhang, Chaofeng Chen, Liang Liao, Chunyi Li, Yixuan Gao, Annan Wang, Erli Zhang, Wenxiu Sun, et al. Q-align: Teaching Imms for visual scoring via discrete text-defined levels. *arXiv preprint arXiv:2312.17090*, 2023. 7, 10
- [90] Jay Zhangjie Wu, Yixiao Ge, Xintao Wang, Stan Weixian Lei, Yuchao Gu, Yufei Shi, Wynne Hsu, Ying Shan, Xiaohu Qie, and Mike Zheng Shou. Tune-a-video: One-shot tuning of image diffusion models for text-to-video generation. In *Proceedings of the IEEE/CVF International Conference on Computer Vision*, pages 7623–7633, 2023. 2
- [91] Xiaoshi Wu, Yiming Hao, Keqiang Sun, Yixiong Chen, Feng Zhu, Rui Zhao, and Hongsheng Li. Human prefer-

- ence score v2: A solid benchmark for evaluating human preferences of text-to-image synthesis, 2023. [11](#)
- [92] Jinglin Xu, Yongming Rao, Xumin Yu, Guangyi Chen, Jie Zhou, and Jiwen Lu. Finediving: A fine-grained dataset for procedure-aware action quality assessment. In *Proceedings of the IEEE/CVF Conference on Computer Vision and Pattern Recognition (CVPR)*, pages 2949–2958, 2022. [7](#), [10](#)
- [93] Jiazheng Xu, Xiao Liu, Yuchen Wu, Yuxuan Tong, Qinkai Li, Min Ding, Jie Tang, and Yuxiao Dong. Imagereward: Learning and evaluating human preferences for text-to-image generation. In *Advances in Neural Information Processing Systems*, 2023. [11](#)
- [94] Shengming Yin, Chenfei Wu, Huan Yang, Jianfeng Wang, Xiaodong Wang, Minheng Ni, Zhengyuan Yang, Linjie Li, Shuguang Liu, Fan Yang, et al. Nuwa-xl: Diffusion over diffusion for extremely long video generation. *arXiv preprint arXiv:2303.12346*, 2023. [2](#)
- [95] Zhenqiang Ying, Haoran Niu, Praful Gupta, Dhruv Mahajan, Deepti Ghadiyaram, and Alan Bovik. From patches to pictures (paq-2-piq): Mapping the perceptual space of picture quality. In *Proceedings of the IEEE/CVF conference on computer vision and pattern recognition*, pages 3575–3585, 2020. [3](#)
- [96] Zhenqiang Ying, Maniratnam Mandal, Deepti Ghadiyaram, and Alan Bovik. Patch-vq: ‘patching up’ the video quality problem. In *Proceedings of the IEEE/CVF Conference on Computer Vision and Pattern Recognition (CVPR)*, pages 14019–14029, 2021. [3](#), [7](#), [9](#)
- [97] Xumin Yu, Yongming Rao, Wenliang Zhao, Jiwen Lu, and Jie Zhou. Group-aware contrastive regression for action quality assessment. In *Proceedings of the IEEE/CVF International Conference on Computer Vision (ICCV)*, pages 7919–7928, 2021. [7](#), [10](#)
- [98] Shenghai Yuan, Jinfa Huang, Yujun Shi, Yongqi Xu, Ruijie Zhu, Bin Lin, Xinhua Cheng, Li Yuan, and Jiebo Luo. Magictime: Time-lapse video generation models as metamorphic simulators. *arXiv preprint arXiv:2404.05014*, 2024. [3](#), [2](#), [7](#)
- [99] Ling-An Zeng, Fa-Ting Hong, Wei-Shi Zheng, Qi-Zhi Yu, Wei Zeng, Yao-Wei Wang, and Jian-Huang Lai. Hybrid dynamic-static context-aware attention network for action assessment in long videos. In *Proceedings of the 28th ACM International Conference on Multimedia*, page 2526–2534, New York, NY, USA, 2020. Association for Computing Machinery. [7](#), [10](#)
- [100] Yan Zeng, Guoqiang Wei, Jiani Zheng, Jiabin Zou, Yang Wei, Yuchen Zhang, and Hang Li. Make pixels dance: High-dynamic video generation. *arXiv preprint arXiv:2311.10982*, 2023. [2](#)
- [101] Weixia Zhang, Kede Ma, Guangtao Zhai, and Xiaokang Yang. Uncertainty-aware blind image quality assessment in the laboratory and wild. *IEEE Transactions on Image Processing*, 30:3474–3486, 2021. [7](#), [9](#)
- [102] Weixia Zhang, Guangtao Zhai, Ying Wei, Xiaokang Yang, and Kede Ma. Blind image quality assessment via vision-language correspondence: A multitask learning perspective. In *Proceedings of the IEEE/CVF Conference on Computer Vision and Pattern Recognition (CVPR)*, pages 14071–14081, 2023. [7](#), [9](#)
- [103] Zhichao Zhang, Xinyue Li, Wei Sun, Jun Jia, Xiongkuo Min, Zicheng Zhang, Chunyi Li, Zijian Chen, Puyi Wang, Zhongpeng Ji, et al. Benchmarking aigc video quality assessment: A dataset and unified model. *arXiv preprint arXiv:2407.21408*, 2024. [7](#), [10](#)
- [104] Daquan Zhou, Weimin Wang, Hanshu Yan, Weiwei Lv, Yizhe Zhu, and Jiashi Feng. Magicvideo: Efficient video generation with latent diffusion models. *arXiv preprint arXiv:2211.11018*, 2022. [2](#)

# Human-Activity AGV Quality Assessment: A Benchmark Dataset and an Objective Evaluation Metric

## Supplementary Material

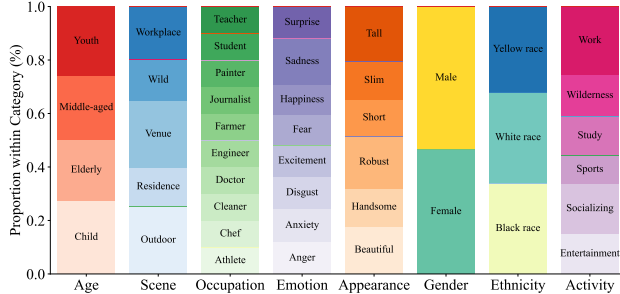


Figure 7. The distribution of 44 subcategories in 8 categories of the 400 prompts.

In this supplementary file, we provide more details of *Human-AGVQA* dataset in Section 7, including text prompts selection, T2V model details, and subjective assessment experiments. We then provide data processing details and further analysis in Section 8, including MOS analysis for T2V models, distortion identification analysis, and the relationship between distortion identification and visual quality. The detailed experiment results are discussed in Section 9, including evaluation criteria in our experiments, compared quality metrics in the proposed benchmark, training details of proposed GHVQ metric, and ablation study of different backbones.

## 7. Human-AGVQA Dataset

### 7.1. Text Prompts Selection

To ensure that the text prompts in our dataset encompass a wide range of real-world human activities, we perform a comprehensive and systematic classification of the words used to create human activity-oriented text prompts. Specifically, we first divide the words into 8 categories according to their properties: *ages, genders, races, occupations, scenes, emotion, appearance, and activities*. Each of these categories is then further subdivided into more specific subcategories that are commonly observed in daily human life, as illustrated in Table 4.

Some example text prompts and their corresponding generated videos are illustrated in Figure 9. The proportions of each subcategory within their respective categories are illustrated in Figure 7. It can be observed that the proportions of subcategories in the *age, occupation, gender, and ethnicity* categories are identical. While for other categories, the subcategories *venue* and *outdoor* in *scene*, *sadness* in *emotion*, *robust* in *appearance*, and *work* and *socializing* in

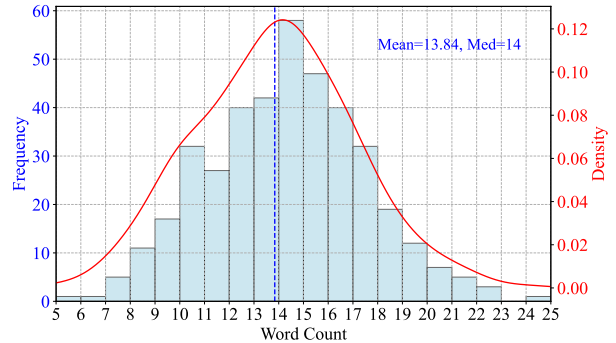


Figure 8. Histogram and density plot of word count per prompt.

*activity* have larger proportions than their respective subcategories. In addition, we analyzed the length of text prompts in the *Human-AGVQA* dataset, and the distribution of word counts are presented in Figure 8. The average text prompt length is 13.85, with a median of 14 words.

### 7.2. T2V models

Detailed information about eight T2V methods is presented in Table 5. All selected T2V models have been published within the past two years and represent the most advanced video generation capabilities of T2V models to date. Except for VideoCrafter2, the resolution of videos generated by these models is at least 512, indicating high clarity. However, the frame rates of StreamingT2V, Latte, and AnimateDiff are below 10 fps, which may result in low motion consistency in actions.

### 7.3. Subjective Quality Assessment Experiments

#### 7.3.1. Visual Quality Scoring Criteria

The quality scores of AGVs are rated from three dimensions: *human appearance quality, action continuity quality, and overall video quality*. Participants rate each dimension on a scale from 1 to 5, where 1 represents the lowest quality and 5 represents the highest. For each dimension, the detailed rating criteria are listed as follows:

#### – Human Appearance Quality

- **5 (Excellent):** The human appearance in the video is **highly realistic, detailed, and perfectly matches the prompt description**. Facial features, body proportions, and skin textures are sharp, clear, and lifelike. Clothing details are well-defined, with no visible distortions, blurring, or artifacts. The overall appearance is completely

Table 4. Subcategories of *ages, genders, races, occupations, scenes, emotion, appearance, and activities*.

Category	Subcategories
age	child, youth, middle-aged, elderly
gender	male, female
scene	outdoor, residence, venue, wild, workplace
appearance	tall, slim, short, handsome, robust, beautiful
occupation	teacher, doctor, engineer, journalist, chef, painter, farmer, athlete, cleaner, student
emotion	happiness, sadness, surprise, anger, fear, anxiety, excitement, disgust
ethnicity	white race, yellow race, black race
activity	study, work, socializing, entertainment, wilderness, sports

consistent with the prompt, including attributes like age, gender, or specific physical traits described.

- **4 (Good):** The human appearance is **generally realistic and matches the majority of the prompt description**. Facial details and body proportions are clear, but some finer details may be missing. Slight blurring or mild artifacts may occasionally appear but do not significantly detract from the realism. Minor deviations from the prompt description (*e.g.*, subtle inconsistencies in age or clothing details) may be present but remain acceptable.
- **3 (Fair):** The human appearance shows **noticeable flaws but still conveys the general idea described in the prompt**. Facial features and body details are somewhat blurred or distorted, and artifacts appear more frequently. The appearance partially matches the prompt, but certain elements (*e.g.*, age, clothing, or specific features) may be misrepresented or missing.
- **2 (Poor):** The human appearance is **highly unrealistic or inconsistent with the prompt description**. Facial features and body proportions are poorly defined, with frequent blurring, distortion, or unnatural textures. Key aspects of the prompt (*e.g.*, age, gender, or specific traits) are misrepresented or missing entirely, reducing the video’s relevance and realism.
- **1 (Bad):** The human appearance is **unrecognizable, highly distorted, or completely missing from the video, which is inconsistent with the prompt**. Facial and body details are absent or severely flawed. If the video does not contain any human body parts (despite the prompt requiring them), this score is set to 1.

#### – Action Continuity Quality

- **5 (Excellent):** Actions are **smooth, natural, and perfectly aligned with the prompt description throughout the video**. Movements are logical, continuous, and free

Table 5. Video formats generated by the eight T2V models in the *Human-AGVQA* dataset.

Methods	Open Source	Year	Duration (s)	FPS	Resolution
Latte [55]	✓	2023	2.0	8	512 × 512
AnimateDiff [22]	✓	2023	2.0	8	512 × 512
Gen-2 [16]	✗	2023	4.0	24	1408 × 768
VideoCrafter2 [9]	✓	2024	1.6	10	512 × 320
MagicTime [98]	✓	2024	2.1	23	512 × 512
StreamingT2V [26]	✓	2024	5.0	8	1280 × 720
Open-sora-plan [40]	✓	2024	2.7	24	512 × 512
StableVideo [1]	✗	2024	4.0	24	1024 × 576

from any interruptions or jerks. The interaction between humans and the environment or objects (if applicable) is realistic and seamlessly integrated. The video fully reflects the activities described in the prompt.

- **4 (Good):** Actions are **generally smooth and align well with the prompt, though minor inconsistencies or occasional interruptions in movement may be present**. Slight jerks or subtle deviations from the described actions occur but do not disrupt the overall continuity or viewing experience.
- **3 (Fair):** Actions show **noticeable flaws in continuity and may partially align with the prompt description**. Jerky movements, illogical transitions, or interruptions are more frequent, reducing the fluidity of the motion. Some actions described in the prompt may be misrepresented or incomplete.
- **2 (Poor):** Actions are **highly inconsistent or poorly aligned with the prompt**. Frequent interruptions, jerks, or illogical transitions significantly disrupt the flow of movement. Actions may be missing key elements or appear unnatural in the context of the prompt.
- **1 (Bad):** Actions are **disjointed, illogical, or completely unrelated to the prompt description**. Movements are erratic and fail to convey the intended activity. If the video does not contain any human body parts (despite the prompt requiring them), this score is set to 1.

#### – Overall Video Quality

- **5 (Excellent):** The video quality is **outstanding, with high sharpness, vibrant colors, stable playback, and well-balanced lighting throughout**. The overall presentation is highly realistic, consistent, and engaging. The content perfectly matches the prompt in terms of both context and visual quality. There are no distortions or artifacts, and all details align with the intended description.
- **4 (Good):** The video quality is **generally high, with minor imperfections such as slight blurring, small artifacts, or occasional lighting inconsistencies**. The content mostly matches the prompt description, with only minor deviations or omissions. These issues do not significantly detract from the overall viewing experience.

	Age	Scene	Occupation	Emotion	Appearance	Gender	Ethnicity	Activity
	Children jump and cheer after receiving long-awaited gifts.	In the rain, an elderly person squats at a street corner, holding a yellowed letter.	A slim male chemical engineer is conducting chemical experiments in the laboratory, wearing protective gear.	In the hospital waiting area, elderly people anxiously watch the display screen.	A beautiful female tea farmer is picking tea in the tea garden.	A beautiful female chef is exploring street food while traveling.	A handsome black journalist is interviewing stars and directors at a film festival.	A slim female cyclist speeds down the track.
Latte								
AnimateDiff								
Gen-2								
VideoCrafter2								
MagicTime								
StreamingT2V								
Open-sora-plan								
StableVideo								

Figure 9. Some example frames of 8 text categories and 8 T2V models in proposed *Human-AGVQA* dataset.

- **3 (Fair):** The video quality is moderate, with noticeable flaws such as blurring, frequent artifacts, or inconsistent lighting. The prompt and video content partially align, but some key details may be missing or misrepresented. These issues reduce the overall coherence and impact of the video.
- **2 (Poor):** The video quality has significant issues, such as severe blurring, persistent artifacts, or poorly bal-

anced lighting. The prompt and video content show weak alignment, with key elements missing or misinterpreted. These flaws make the video difficult to watch and significantly reduce its realism and coherence.

- **1 (Bad):** The video quality is extremely poor, with pervasive distortions, blurring, or lighting problems. The video content is almost entirely inconsistent with the prompt, failing to deliver the intended description. The



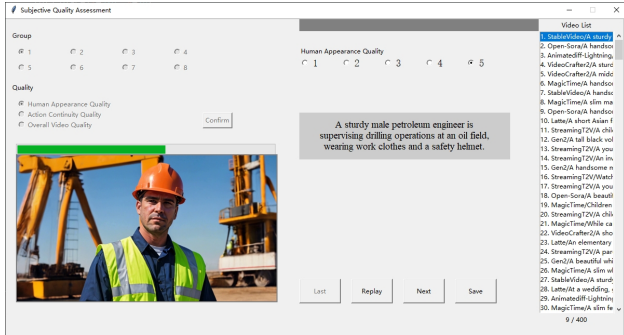


Figure 10. Annotation Interface for Subjective Quality Experiment.

video is barely watchable and lacks any sense of coherence.

### 7.3.2. Semantic Distortion Identification Criteria

#### – Human Body Presence

- **1 (Present)** A body part is labeled as *present* if its **outline or general** shape can be observed in the video, even if **fine details are unclear** due to distortion (e.g., blurry facial features or stiff limb movements). For example, the overall outline of the face is distinguishable, the arms are reasonably connected to the torso, and the shapes of the legs and feet are visible. Even minor proportional inconsistencies or blurriness do not disqualify a body part from being labeled as present.
- **0 (Not Present)** A body part is labeled as *absent* if it is **entirely missing** from the video (e.g., obscured, generation failure, or no relevant features are displayed) or if severe quality issues make its **outline or shape unrecognizable** (e.g., when the background and the body part are **indistinguishable**). For instance, if the face cannot be separated from the background, the arms or legs are entirely absent, or the feet are fused with the ground to an indistinguishable degree, the body part is considered absent.

#### – Human Body Distortion

- **1 (Distorted)** A body part is labeled as *distorted* if it shows significant quality issues. Examples include **blurry** facial features, **disproportionate or distorted shapes**, **compression artifacts**, arms with **unnatural movements** or **disconnection from the torso**, a torso with **abnormal proportions** or **missing details**, legs that appear **broken, stretched**, or **disproportionate**, and feet with **unnatural shapes, incorrect positions, or unnatural interactions** with the ground (e.g., floating or penetrating the surface).
- **0 (No Distortion)** A body part is labeled as *no distortion* if it appears **clear, natural**, and **consistent** with the overall video. For example, facial features are proportionate,

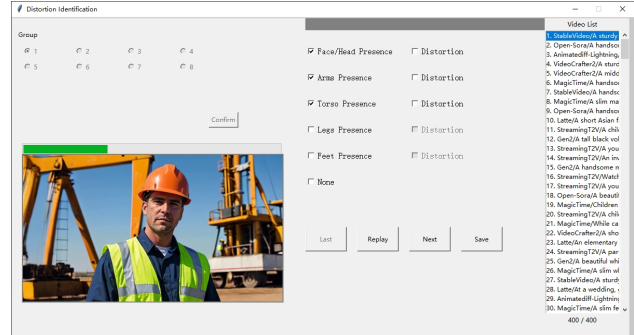


Figure 11. Annotation Interface for Distortion Identification.

arm movements are smooth and natural, the torso connects properly with other body parts, and the shapes and motions of the legs and feet align with expected behavior.

### 7.3.3. Subjective Quality Experiment Procedure

A total of 80 subjects participated in the visual quality scoring experiment, with ages ranging from 20 to 30 years. The group included 46 males and 34 females. Given that the semantic artifact identification task is less complex than the visual quality scoring task, we invited 5 experts in the field of AIGC quality assessment to perform the semantic artifact identification. Each video was rated by 10 subjects, and labeled by 5 experts. The annotation interface for subjective quality experiment and distortion identification are shown in Figure 10 and Figure 11.

All subjects had normal or corrected-to-normal vision. The experiments were conducted in a controlled environment according to the recommendations of ITU-R BT.500-13 [2] to minimize external variables that could influence the judgments of the subjects. The setup included 27-inch calibrated display monitors with 95% DCI-P3 color gamut and a resolution of 4K. The viewing distance was set at 70 cm. The room lighting was maintained at a consistent level of 300 lux to ensure uniformity across all viewing sessions.

Before the formal assessments, subjects underwent a training session where they reviewed sample AGVs that were not included in the formal experiment. This session aimed to familiarize them with the evaluation criteria and the rating interface. In the formal experiment, 3,200 videos were divided into eight groups, each containing 400 videos that covered all 400 prompts. To avoid visual fatigue, each session lasted no longer than 30 minutes, ensuring participants could maintain a high level of attention and accuracy in their ratings. In total, there are 96,000 opinion scores and 160,000 binary labels in the *Human-AGVQA* dataset.

## 8. Data Processing and Analysis

We follow the recommended method in [2] to process the subjective ratings collected during the experiment. Outlier

ratings are detected and removed if they deviate by more than  $2\sigma$  (for normal distributions) or  $\sqrt{20}\sigma$  (for non-normal distributions) from the mean rating for that condition. Observers contributing more than 5% of outlier ratings are excluded from the analysis. For each test condition, the mean score ( $\mu_i$ ) and standard deviation ( $\sigma_i$ ) are calculated based on all valid ratings provided by observer  $i$ :

$$\mu_i = \frac{1}{N_i} \sum_{j=1}^{N_i} s_{ij}, \quad \sigma_i = \sqrt{\frac{1}{N_i - 1} \sum_{j=1}^{N_i} (s_{ij} - \mu_i)^2} \quad (9)$$

where  $s_{ij}$  represents the raw rating assigned by observer  $i$  to condition  $j$ , and  $N_i$  is the number of conditions rated by observer  $i$ . To mitigate individual bias, each raw score  $s_{ij}$  is normalized to a Z-score:

$$Z_{ij} = \frac{s_{ij} - \mu_i}{\sigma_i} \quad (10)$$

Finally, the Mean Opinion Score (MOS) for each test condition  $j$  is computed as the average of the normalized Z-scores across all observers ( $M_j$ ):

$$MOS_j = \frac{1}{M_j} \sum_{i=1}^{M_j} Z_{ij} \quad (11)$$

For distortion identification, we use a voting method to determine body presence and body distortion. The label with the highest number of votes is selected as the final result.

### 8.1. Inter-subject Consistency

To evaluate the consistency and reliability of quality scoring, we compute the inter-annotator agreement metric, Krippendorff’s Alpha ( $\alpha$ ), where Krippendorff’s Alpha ( $\alpha$ ) for HA quality, AC quality, OV quality are 0.708, 0.695, and 0.628, respectively, indicating appropriate variations among subjects.

For semantic distortion identification, we calculated the proportions of options receiving 3 votes, 4 votes, and 5 votes, which were 9.7%, 41.5%, and 46.4%, respectively. This demonstrates that the majority of the votes from subjects were consistent.

### 8.2. MOS Analysis for Each T2V Model

We analyzed the MOS of three quality dimensions across 44 attributes (mentioned in Table 4) for eight T2V models (mentioned in Table 5), as shown in Figure 12.

**StableVideo.** Overall video (OV) quality emerges as the **strongest aspect** of StableVideo, consistently achieving **high scores** on most attributes, including complex *scenarios* such as *workplace* and *emotion* like *anger*. This highlights the model’s **robust capability** to generate visually coherent outputs. Human appearance (HA) quality

also performs well, though it *slightly lags behind* overall video quality, indicating the model’s ability to generate **clear and recognizable** human features but with room for **improvement** compared to its overall visual performance. In contrast, action continuity (AC) quality represents the **model’s primary weakness**, consistently scoring the **lowest** among the three dimensions. This is particularly evident in subcategories requiring complex movements or high dynamism, such as *surprise* in *emotion* and *sports* in *activity*, revealing the model’s limitations in modeling motion continuity.

**AnimateDiff.** The AnimateDiff model **excels in AC Quality**, particularly in *emotion* and *activity*, where it **consistently outperforms** the other quality dimensions. This demonstrates the model’s **strength** in generating **continuous and coherent motion**. OV Quality shows stable and relatively **high performance** across most attributes, reflecting the model’s ability to maintain overall visual consistency. However, HA Quality **falls behind**, especially in categories such as *occupation* and *activity*, where the model struggles with **rendering detailed and realistic** human appearances. These findings suggest that while AnimateDiff is highly competent in motion continuity, it faces challenges in producing visually intricate details.

**Gen-2.** The Gen-2 model demonstrates **exceptional performance** in OV Quality, consistently achieving the **highest scores** across all subcategories. This underscores the model’s **strength** in generating visually cohesive outputs. HA Quality ranks second, showing a **stable and strong ability** to generate **clear and recognizable** human features, although it *slightly trails* OV Quality. AC Quality, however, is the **weakest** of the three dimensions, particularly in subcategories involving **complex movements**, such as *angry* in *emotion* and *sports* in *activity*, where it exhibits noticeable limitations.

**Latte.** Latte shows **only average performance** in terms of OV quality, but it is still slightly insufficient compared with other models. AC Quality exhibits greater variability, with **strong performance** in categories like *sadness* and *surprise*, but struggles in more complex occupational categories. HA Quality is the **weakest dimension**, particularly in *occupation* and *activity* categories, where the model demonstrates **limitations** in generating **detailed and realistic** human appearances. These observations suggest that the Latte model performs moderately well in maintaining overall video quality, its capacity to generate fine-grained human details requires further improvement.

**MagicTime.** MagicTime **performs poorly** in AC quality among the three quality scores, and there is a **certain gap compared with other models**. In addition, **HA quality consistently underperforms**, especially in categories

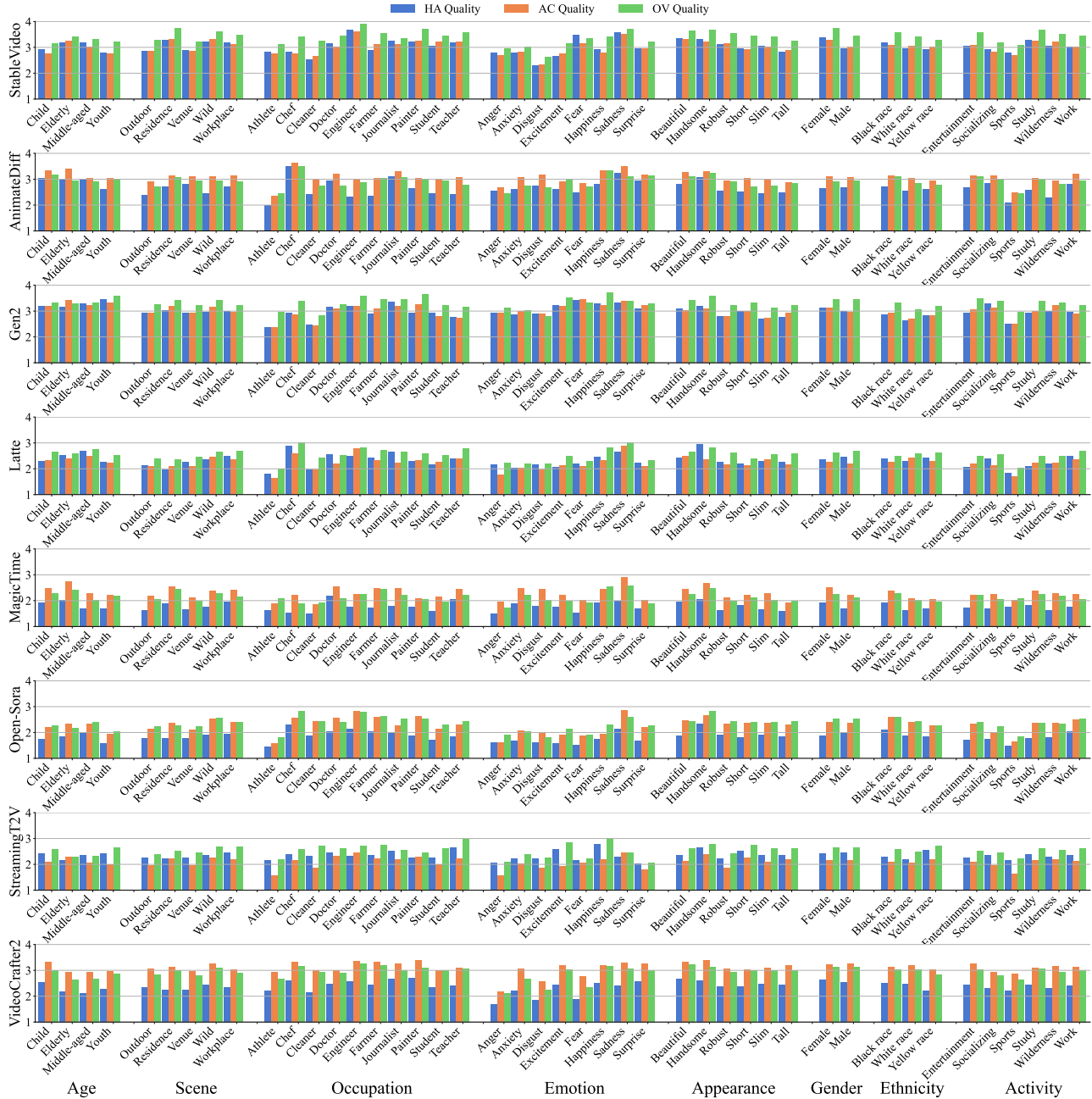


Figure 12. The MOS comparison for 8 text categories of each T2V model.

involving complex emotions, movements, or appearances, highlighting the model’s limitations in rendering detailed human features. The model shows **balanced performance** in categories like *scene* and *gender* but exhibits significant variability in *occupation* and *appearance*, indicating its inconsistent generation quality depending on the attribute.

**Open-Sora.** The performance of OV Quality and AC Quality is **not satisfactory**, and they still **fall short significantly**

**compared to other models.** In addition, HA quality consistently **lags behind**, particularly in the *occupation*, *emotion*, and *activity* categories, where the model struggles to render detailed and realistic human appearances. These results suggest that while Open-Sora excels in visual consistency and motion continuity, it faces challenges in human appearance generation.

**StreamingT2V.** StreamingT2V shows **only average per-**

Table 6. The total and proportion of occurrences and distortions for body parts in the 400 videos generated by each model. Red represents the minimum value in a column.

Models	Occurrences / Distortions					
	Face	Arms	Torso	Legs	Feet	None / Total
Latte [55]	358 / 250 89.5 / 69.8	324 / 310 81.0 / 95.7	329 / 140 82.3 / 42.6	89 / 56 22.3 / 62.9	48 / 38 12.0 / 79.2	21 / 794 5.2 / 69.2
AnimateDiff [22]	373 / 245 93.2 / 65.7	352 / 316 88.0 / 89.8	357 / 88 89.2 / <b>24.6</b>	183 / 67 45.8 / <b>36.6</b>	108 / 63 27.0 / <b>58.3</b>	22 / 779 5.5 / <b>56.7</b>
Gen-2 [16]	383 / 250 95.8 / <b>65.3</b>	357 / 329 89.2 / 92.2	361 / 134 90.2 / 37.1	138 / 86 34.5 / 62.3	93 / 72 23.3 / 77.4	10 / 871 2.5 / 65.4
StreamingT2V [26]	361 / 304 90.2 / 84.2	366 / 342 91.5 / 93.4	348 / 199 87.0 / 57.2	170 / 127 42.5 / 74.7	105 / 92 26.3 / 87.6	15 / 1064 3.7 / 78.8
VideoCrafter2 [9]	382 / 324 95.5 / 84.8	350 / 295 87.5 / <b>84.3</b>	365 / 117 91.2 / 32.1	98 / 60 24.5 / 61.2	64 / 49 16.0 / 76.6	11 / 845 2.8 / 67.1
Open-sora-plan [40]	379 / 333 94.8 / 87.9	376 / 371 94.0 / 98.7	367 / 214 91.7 / 58.3	134 / 84 33.5 / 62.7	68 / 60 17.0 / 88.2	9 / 1062 2.2 / 80.2
MagicTime [98]	320 / 292 80.0 / 91.2	309 / 302 77.2 / 97.7	303 / 177 75.7 / 58.4	248 / 177 62.0 / 71.4	216 / 187 54.0 / 86.6	66 / 1135 16.5 / 81.3
StableVideo [1]	393 / 289 98.3 / 73.5	378 / 323 94.5 / 85.4	381 / 127 95.3 / 33.3	128 / 60 32.0 / 46.9	72 / 47 18.0 / 65.3	2 / 846 <b>0.5</b> / 62.6

**formance** in terms of OV quality and HA quality, indicating its **limited capability** to generate sufficiently detailed human appearances. However, it **falls short in AC quality**, particularly in dynamic categories such as *occupation* (*Athlete* and *Cleaner* and *emotion* (*surprise* and *anger*), where the scores are significantly lower. These findings indicate that while StreamingT2V is effective in static scenarios, its handling of motion continuity in dynamic contexts requires further improvement.

**VideoCrafter2.** VideoCrafter2 shows **balanced performance in OV quality and AC quality**, with stable scores across most attributes. However, HA quality consistently underperforms, particularly in *emotion* categories such as *anger* and *disgust*, and *activity* categories such as *sports* and *work*, where it significantly trails OV and AC quality. These results **highlight the model’s limitations** in generating detailed and realistic human appearances. Nevertheless, the model demonstrates **balanced performance** in categories like *age*, *scene*, *ethnicity*, and *gender*, reflecting its comprehensive generation capability in these areas. However, its inconsistent performance in *emotion*, particularly in attributes like *anger* and *disgust*, underscores the challenges it faces in modeling complex emotional details.

### 8.3. Distortion Identification Analysis

We calculate the proportion of occurrences and distortions for each body part of AGVs for different T2V models, as detailed in Table 6. For body occurrences, StableVideo performs the best, with the highest proportion of main body parts (face, arms, torso) present among these T2V models, and only 0.5% of videos generated by StableVideo lack any human depiction. In contrast, MagicTime performs the worst, with 16.5% of videos missing any human body

parts. In terms of distortions, AnimateDiff and StableVideo exhibit better performance, with VideoCrafter2 and Gen-2 also showing comparable results. In contrast, Open-Sora and MagicTime show significant deficiencies, with distortions in certain body parts accounting for over 95%. These findings closely align with the subjective quality scores of corresponding T2V models.

Moreover, an observation of significant concern is that 16.5% of videos generated by MagicTime lack any depiction of human body parts, indicating a shortfall in the model’s ability to maintain consistency between textual descriptions and visual content. StableVideo demonstrates the most robust performance in this regard.

### 8.4. The Relationship between Semantic Distortion Identification and Visual Quality Scoring

We calculated the correlation between the three subjective quality scores and the distortion identification labels, as shown in Figure 13. Notably, when analyzing the relationship between body part distortions and quality scores, we included only videos in which the corresponding body part was present. For example, in assessing the correlation between facial distortion and quality scores, we considered only videos where a face was visible.

#### 8.4.1. Body Parts Distortion

Overall, the quality of T2V models across the three evaluated dimensions demonstrates a certain degree of correlation with the distortions in the five body parts. Among these, facial distortion has the most significant impact on human appearance quality, followed by distortions in the torso and legs. This pattern aligns with the natural human perception process, which prioritizes facial recognition before focusing on the torso and other body parts.

Of the three quality dimensions, HA Quality exhibits the strongest correlation with body part distortions, followed by AC Quality, with OV Quality showing the weakest correlation. This suggests that body part distortions most directly influence perceptions of human appearance quality, with a lesser effect on the continuity of human actions, and the least impact on overall video quality.

Interestingly, for certain models, such as VideoCrafter2, quality scores show a negative correlation with distortions in the arms and feet. This implies that viewers’ attention is drawn more to prominent areas like the face and torso, making distortions in less visually critical body parts less influential.

#### 8.4.2. Body Parts Presence

We also calculated the correlation between the presence of five body parts and the subjective quality scores. The results indicate that the presence of a face significantly impacts video quality, followed by the torso. This may be attributed to the design of the subjective experiment, where

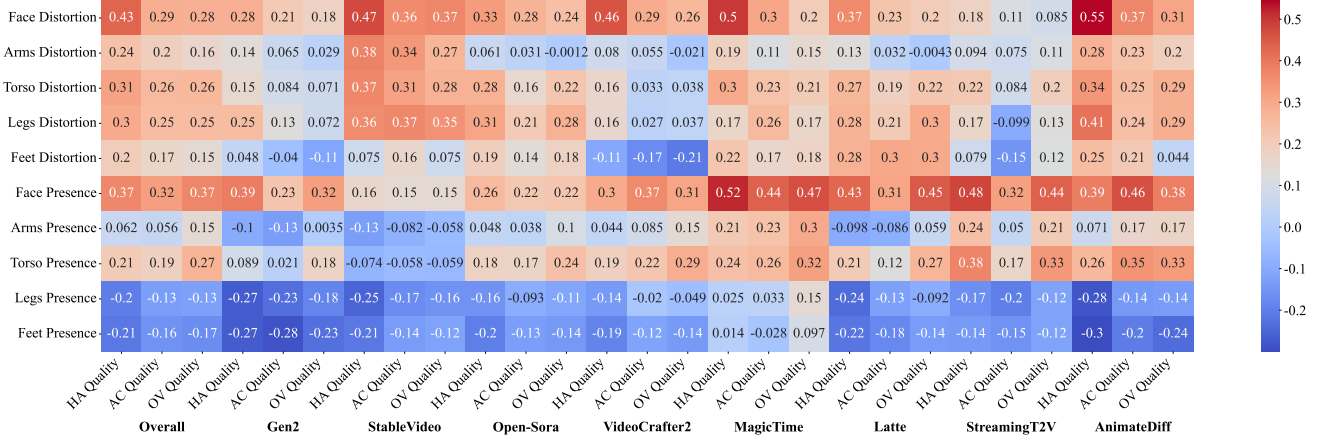


Figure 13. The correlation between the semantic distortion identification and subjective quality.

videos with no visible human parts were assigned the lowest HA and AC quality scores (1 point). Moreover, in most cases, if the face (head) is absent, other body parts are also missing.

For the MagicTime model, its quality scores show a strong correlation with the presence of a face, with the HA score reaching as high as 0.52. This suggests that the presence of a face plays a crucial role in determining the quality scores for videos generated by MagicTime. Conversely, it also indicates that MagicTime frequently generates videos without human faces, consistent with our findings in Table 6.

Interestingly, the presence of legs and feet often correlates negatively with all three quality dimensions, suggesting that their inclusion tends to degrade overall video quality. This underscores the current limitations of T2V models in accurately generating human legs and feet, as distortions in these areas significantly impact viewers' subjective perception of video quality across all dimensions.

## 9. Experiment Settings

### 9.1. Evaluation Metrics

Spearman Rank Correlation Coefficient (SRCC) and Pearson Linear Correlation Coefficient (PLCC) are widely utilized metrics to quantify the relationship between predicted scores and ground truth scores. SRCC measures the monotonic relationship between two variables by comparing their rank orders. Unlike metrics that assume linearity, SRCC is robust to non-linear relationships, making it particularly well-suited for assessing relative rankings. It is mathematically defined as:

$$SRCC = 1 - \frac{6 \sum_{n=1}^N (v_n - p_n)^2}{N(N^2 - 1)}, \quad (12)$$

where  $N$  denotes the number of data points,  $v_n$  represents the rank of the  $n$ -th ground truth score, and  $p_n$  represents the rank of the corresponding predicted score. The value of SRCC ranges from 0 to 1, with 1 indicating a perfect monotonic increasing relationship, and 0 signifying the absence of any monotonic relationship. In the context of quality assessment, a high SRCC indicates that the predicted rankings are well-aligned with the rankings of ground truth scores, reflecting the model's ability to capture the subjective perception of quality differences.

In contrast, the Pearson Linear Correlation Coefficient (PLCC) measures the strength of the linear correlation between predicted and ground truth scores, focusing on how closely the predicted values align with the true scores in absolute terms. It is expressed as:

$$PLCC = \frac{\sum_{n=1}^N (y_n - \bar{y})(\hat{y}_n - \bar{\hat{y}})}{\sqrt{\sum_{n=1}^N (y_n - \bar{y})^2 \sum_{n=1}^N (\hat{y}_n - \bar{\hat{y}})^2}}, \quad (13)$$

where  $y_n$  and  $\hat{y}_n$  denote the  $n$ -th ground truth and predicted scores, respectively, and  $\bar{y}$  and  $\bar{\hat{y}}$  are their corresponding means. Like SRCC, PLCC also ranges from 0 to 1, where 1 indicates a perfect positive linear correlation and 0 denotes no linear relationship. Unlike SRCC, which evaluates relative rankings, PLCC assesses the accuracy of predicted scores with respect to their numerical values, making it a critical metric for evaluating absolute predictive precision.

### 9.2. Compared Quality Metrics

#### 9.2.1. Image Quality Assessment Methods

In all the IQA methods mentioned below, we uniformly extract 8 frames from each video in the *Human-AGVQA* dataset. These frames are then fed into the corresponding IQA methods to obtain 8 quality scores, and the average of these scores is taken as the method's output.

**NIQE** [58] is a no-reference image quality assessment (IQA) model that evaluates the quality of images based on natural scene statistics (NSS) without relying on human-rated training data. For the *Human-AGVQA* dataset, we applied NIQE to assess image quality using selected video frames.

**BRISQUE** [57] leverages directional contrast features extracted from the Curvelet domain to assess the quality of contrast-distorted images. For the *Human-AGVQA* dataset, we utilized this approach to evaluate image quality based on its directional contrast features.

**HyperIQA** [68] introduces a self-adaptive hyper network for blind image quality assessment (BIQA) in the wild, addressing diverse content and distortion types in real-world images. For the *Human-AGVQA* dataset, we applied HyperIQA to assess image quality by adaptively learning perception rules and predicting quality scores.

**UNIQUE** [101] is a unified uncertainty-aware BIQA model designed to handle synthetic and realistic distortions. The model predicts both quality scores and associated uncertainties, enabling a probabilistic interpretation of image quality. For the *Human-AGVQA* dataset, we used UNIQUE to assess video frame quality based on its learning-to-rank framework.

**MUSIQ** [34] introduces a multi-scale image quality Transformer designed to handle full-resolution images with varying sizes and aspect ratios. The model uses hash-based 2D spatial embedding and scale embedding to capture positional and scale information effectively. For the *Human-AGVQA* dataset, we applied MUSIQ to evaluate video frame quality by leveraging its multi-scale feature extraction capability.

**StairIQA** [72] introduces a staircase network that integrates features from multiple convolutional layers of a CNN to capture better both low-level visual details and high-level semantic information for in-the-wild image quality assessment. For the *Human-AGVQA* dataset, we used the official implementation and adopted this approach to evaluate image quality without modifications.

**CLIP-IQA** [81] is a visual perception assessment model that utilizes the pre-trained CLIP framework to evaluate both the quality and abstract attributes of images. It introduces an antonym prompt pairing strategy (e.g., *Good photo* vs. *Bad photo*) to mitigate linguistic ambiguity and employs cosine similarity to predict image quality scores. For the *Human-AGVQA* dataset, we used the official implementation, applying CLIP-IQA to assess video frame quality.

**LIQE** [102] is a multitask learning framework for blind image quality assessment (BIQA) that leverages vision-

language correspondence. LIQE uses CLIP for feature embeddings and optimizes tasks jointly by marginalizing probabilities over a textual template that describes scene, distortion, and quality. For the *Human-AGVQA* dataset, we used the official implementation, applying the quality assessment textual template to evaluate the video frame quality.

**MA-AGIQA** [84] introduces a framework for AI-generated image quality assessment by combining large multi-modality models (LMMs) with traditional deep neural networks (DNNs). For the *Human-AGVQA* dataset, we used the official implementation, applying MA-AGIQA to evaluate the video frame quality without modifications.

### 9.2.2. Video Quality Assessment Methods

**TLVQM** [38] is a two-level video quality model that first computes low-complexity features across the entire video and then selects representative frames based on these features to extract high-complexity features.

**RAPIQUE** [78] is a video quality assessment model that combines spatial-temporal scene statistics with high-level features extracted using deep CNNs. For the *Human-AGVQA* dataset, we used the official implementation, applying sparse frame sampling and integrating spatial and temporal features to evaluate video quality.

**VIDEVAL** [77] applies a feature selection strategy based on efficient blind VQA models. Using the official open-source code, we converted *Human-AGVQA* videos from RGB to YUV420 format for feature extraction.

**Patch-VQ** [96] is a video quality model that extracts spatial and temporal features from video frames and patches to analyze the relationship between local distortions and overall video quality. For the *Human-AGVQA* dataset, we used Patch-VQ’s official implementation, dividing each video into space-time patches for feature extraction and quality prediction.

**SimpleVOA** [71] uses an end-to-end network to extract spatial features directly from video frames and motion features to capture temporal distortions. A pre-trained Slow-Fast model processes 8 uniformly sampled frames rescaled to a height of 520. We used the official SimpleVOA model and finetuned it on *Human-AGVQA*.

**FAST-VQA** [87] introduces a grid mini-patch sampling (GMS) strategy to balance local quality assessment with global context while reducing computational costs for high-resolution videos. We used the official FAST-VQA-B model and finetuned it on *Human-AGVQA*.

**DOVER** [88] is a video quality evaluator that assesses quality from technical and aesthetic perspectives. We used the official code without modifications.

Table 7. Details of the model structure for the proposed model.

Training Hyper-Parameters	Name/Value	More Information
Action Quality Analyzer	SlowFast-R50	parameter size: 34M
Holistic Quality Feature	PickScore	backbone: CLIP-ViT-H/14
Human body-part segmentation	Spaiens	parameter size: 2B
Human appearance feature	shallow hourglass	parameter size: 56M
Text Feature Extraction	PickScore	backbone: CLIP-ViT-H/14

**T2VQA** [39] is a transformer-based model designed to evaluate text-to-video quality, focusing on text-video alignment and video fidelity. It uses BLIP and Swin-T for feature extraction, followed by feature fusion through a cross-attention module and quality regression using a large language model. On the *Human-AGVQA* dataset, we used the official T2VQA model and finetuned it on *Human-AGVQA*.

**UGVQ** [103] is a unified framework for video quality assessment, focusing on spatial quality, temporal coherence, and text-to-video alignment. It utilizes features from CLIP for text and visual representations and SlowFast for motion representation. For the *Human-AGVQA* dataset, we employed UGVQ’s feature extraction and fusion modules to evaluate video quality comprehensively across these three dimensions.

**EvalCrafter** [54] is an evaluation framework for text-to-video (T2V) generative models, focusing on video quality, text-video alignment, motion quality, and temporal consistency. It uses a benchmark of 700 prompts and 17 evaluation metrics to analyze T2V model performance. For overall video quality, we directly used implementation code in EvalCrafter on the *Human-AGVQA* dataset without specific changes.

**Q-Align** [89] introduces a methodology for teaching large multi-modality models (LMMs) to assess video quality using discrete text-defined levels such as *excellent*, *good*, and *poor*. It converts mean opinion scores (MOS) into these rating levels for training and infers scores by weighting the predicted probabilities of the levels. For the *Human-AGVQA* dataset, we used the official code for inference without modifications.

### 9.2.3. Action Quality Assessment Methods

**USDL** [74] is an uncertainty-aware score distribution learning approach for action quality assessment (AQA), treating actions as instances associated with score distributions. For the *Human-AGVQA* dataset, since all videos contain more than 16 frames, each video is evenly divided into ten segments. Feature extraction is performed using an I3D backbone pre-trained on Kinetics. The final scores are normalized linearly, scaling the raw scores based on their minimum and maximum values to a range of [0, 100]. These normal-

Table 8. Details of the hyper-parameters for the model training.

Training Hyper-Parameters	Name/Value
frame sampling for SQA	8
frame resolution for SQA	$512 \times 512$
frame resolution for AQA	$256 \times 256$
batch size (videos)	16
lr max	$1e - 5$
lr schedule	StepLR
decay ratio	0.9
decay interval	5
numerical precision	float32
epoch	30
optimizer	Adam

ized scores are then used to construct Gaussian distributions with the normalized value as the mean.

**ACTION-NET** [99] is a hybrid attention network tailored for action quality assessment (AQA) in long videos. It combines dynamic video information with static postures of action subjects in selected frames. For the dynamic stream, frames are sampled at a rate of 4 frames per second. For the static stream, the first, middle, and last frames are sampled, and the action subjects are cropped using the original detection algorithm.

**CoRe** [97] evaluates action quality by regressing relative scores against a reference video with similar attributes, such as action category. Due to differences in categorization strategies between the *Human-AGVQA* and *AQA-7* datasets, we randomly selected an exemplar video generated by another T2V model within the same prompt category. Each video was divided into four equal segments, each containing four consecutive frames.

**TSA** [92] is a temporal segmentation attention module designed for procedure-aware cross-attention learning after spatial-temporal feature extraction. Similar to CoRe, each video is evenly divided into segments of four consecutive frames and processed using the I3D model.

For Motion Smoothness, Temporal Flickering, Action-Score, and Flow-Score metrics, we directly used their respective implementation code in VBench [33] and EvalCrafter [54] without specific changes.

### 9.3. Training details

The detailed structure of the proposed GHVQ metric is provided in Table 7. The corresponding hyperparameters for model training are listed in Table 8.

### 9.4. Ablation Study: The Effectiveness of Different Backbones

To further validate the effectiveness of the selected backbone networks, we conducted comparative experiments on four extraction modules: body-part segmentation network,

Table 9. Ablation Study of Body Segmentation Network.

Methods	HA Quality		AC Quality		OV Quality		Distortion Identification	
	SRCC	PLCC	SRCC	PLCC	SRCC	PLCC	Occ	Dis
None	0.659	0.671	0.692	0.704	0.745	0.752	0.581	0.524
OpenPose [4]	0.757	0.764	0.740	0.748	0.753	0.751	0.745	0.667
Deeplabv3+ [10]	0.712	0.725	0.724	0.736	0.758	0.767	0.649	0.546
JPPNet [50]	0.685	0.692	0.726	0.732	0.773	0.782	0.582	0.475
HRNet [69]	0.772	0.783	0.704	0.714	0.763	0.773	0.675	0.588
Sapiens [36]	<b>0.812</b>	<b>0.821</b>	<b>0.788</b>	<b>0.792</b>	<b>0.780</b>	<b>0.788</b>	<b>0.815</b>	<b>0.752</b>

Table 10. Ablation Study of Text Feature Extraction Network.

Methods	HA Quality		AC Quality		OV Quality		Distortion Identification	
	SRCC	PLCC	SRCC	PLCC	SRCC	PLCC	Occ	Dis
None	0.781	0.789	0.754	0.765	0.773	0.776	0.802	0.736
CLIPScore [27]	0.795	0.803	0.758	0.764	0.778	0.778	0.810	0.737
BLIP [45]	0.806	0.812	0.772	0.782	0.768	0.773	0.810	0.744
ViCLIP [85]	0.803	0.807	0.769	0.773	0.767	0.774	0.813	0.739
ImageReward [93]	0.801	0.805	0.775	0.778	0.772	0.779	0.811	0.735
HPSv2 [91]	0.810	0.817	0.779	0.790	<b>0.780</b>	0.787	0.814	0.751
PickScore [37]	<b>0.812</b>	<b>0.821</b>	<b>0.788</b>	<b>0.792</b>	<b>0.780</b>	<b>0.788</b>	<b>0.815</b>	<b>0.752</b>

holistic quality feature extraction network, text feature extraction network, and action quality analyzer.

#### 9.4.1. Body-part Segmentation Network

For the body-part segmentation network, performance differences between methods are more pronounced, as shown in Table 9. Among them, Sapiens achieves the best results in HA and AC Quality. This superior performance can be attributed to Sapiens’ high accuracy in body part segmentation and pose estimation, allowing for precise identification of key body parts and thereby enhancing human appearance quality and action continuity. In contrast, earlier models such as JPPNet and Deeplabv3+ lack the segmentation precision and capability to handle complex poses, leading to weaker performance in overall quality metrics. Sapiens’ strong performance is also reflected in distortion identification.

#### 9.4.2. Holistic Quality Feature Extraction Network

For holistic quality features, PickScore achieves the highest scores across all quality metrics, as shown in Table 11. PickScore effectively captures rich holistic quality features from the input video. Compared to other methods such as CLIPScore, ViCLIP, and CLIP (OpenAI), PickScore’s superior performance suggests that accurate holistic quality feature significantly benefits video quality evaluation. It is worth noting that the performance of HPS v2 and CLIP-H/14 (LAION) is very close to that of PickScore.

#### 9.4.3. Text Feature Extraction Network

For text feature extraction, PickScore achieves the highest scores across all quality metrics, as shown in Table 10. PickScore effectively captures rich semantic information from the input text, providing a more comprehensive con-

Table 11. Ablation Study of Holistic Quality Feature.

Methods	HA Quality		AC Quality		OV Quality		Distortion Identification	
	SRCC	PLCC	SRCC	PLCC	SRCC	PLCC	Occ	Dis
None	0.704	0.722	0.681	0.695	0.727	0.734	0.761	0.710
CLIPScore [27]	0.728	0.739	0.712	0.719	0.743	0.748	0.772	0.717
ViCLIP [85]	0.723	0.731	0.723	0.733	0.732	0.744	0.789	0.731
CLIP-B/16 (OpenAI) [64]	0.726	0.735	0.717	0.728	0.738	0.749	0.792	0.735
CLIP-B/32 (OpenAI) [64]	0.739	0.745	0.731	0.742	0.746	0.752	0.787	0.729
CLIP-L/14 (OpenAI) [64]	0.752	0.757	0.743	0.749	0.751	0.766	0.798	0.740
CLIP-L/14 (LAION) [12]	0.776	0.785	0.768	0.777	0.760	0.768	0.802	0.743
CLIP-H/14 (LAION) [12]	0.799	0.812	0.785	0.791	0.772	0.780	0.811	0.745
CLIP-G/14 (LAION) [12]	0.795	0.805	0.782	0.786	0.768	0.778	0.805	0.737
HPSv2 [91]	0.809	0.814	<b>0.788</b>	0.790	0.779	0.784	0.814	0.750
PickScore [37]	<b>0.812</b>	<b>0.821</b>	<b>0.788</b>	<b>0.792</b>	<b>0.780</b>	<b>0.788</b>	<b>0.815</b>	<b>0.752</b>

Table 12. Ablation Study of Action Quality Analyzer.

Methods	HA Quality		AC Quality		OV Quality		Distortion Identification	
	SRCC	PLCC	SRCC	PLCC	SRCC	PLCC	Occ	Dis
None	0.767	0.770	0.747	0.748	0.728	0.740	0.753	0.704
I3D [5]	0.781	0.789	0.752	0.762	0.709	0.713	0.811	0.739
C3D [76]	0.797	0.798	0.760	0.773	0.709	0.713	0.811	0.739
X3D [18]	0.808	0.812	0.784	0.790	0.764	0.769	0.813	0.747
SlowFast [19]	<b>0.812</b>	<b>0.821</b>	<b>0.788</b>	<b>0.792</b>	<b>0.780</b>	<b>0.788</b>	<b>0.815</b>	<b>0.752</b>

textual understanding of the video content, which plays a critical role in enhancing overall quality assessment. Compared to other methods such as CLIPScore and ViCLIP, PickScore’s superior performance suggests that accurate semantic information significantly benefits video quality evaluation. It is worth noting that the performance of HPS v2 is very close to that of PickScore. PickScore leverages the Pick-a-Pic dataset for training, which is specifically designed to optimize performance on preference comparison tasks. In contrast, HPS v2 is trained on the more extensive HPD v2 dataset, characterized by its larger scale and greater diversity in both image content and preference distributions.

#### 9.4.4. Action Quality Analyzer

For the action quality analyzer, the SlowFast method demonstrates superior performance across all quality metrics, particularly in HA Quality and AC Quality, as shown in Table 12. In comparison, other methods such as I3D and C3D show slightly lower performance. The advantage of SlowFast lies in its ability to capture dynamic features across fast and slow motion, enabling comprehensive temporal information extraction. Additionally, SlowFast achieves the best results in distortion identification, indicating its strong capacity for detecting and recognizing distortions within video content.